LMS/ESL/S15233
ESL-RPT-2018-02

Environmental Sciences Laboratory

Plume Persistence Final Project Report

May 2018

U.S. DEPARTMENT OF ENERGY | Legacy Management

This page intentionally left blank

Contents

Figures

Tables

Appendixes

This page intentionally left blank

Abbreviations

1D	one-dimensional
AFO	amorphous ferric oxyhydroxide
alk	alkalinity
AmmOx	ammonium oxalate leach
amsl	above mean sea level
AS&T	Applied Studies and Technologies
CE	cation exchange
cm	centimeter
disp	dispersion
DOE	U.S. Department of Energy
dual	dual porosity
ESL	Environmental Sciences Laboratory
exch	cation exchange capacity
ft	feet
ft/yr	feet per year
g	grams
gcsd	generic complexation, strong sorption sites, sorption site density
gcsk	generic complexation, strong sorption sites, log equilibrium constant
gcssd	generic complexation, super strong sorption sites, sorption site density
gcssk	generic complexation, super strong sorption sites, log equilibrium constant
gyp	gypsum
h	hours
kg	kilograms
L	liters
LM	Office of Legacy Management
MCL	maximum contaminant level
µg	micrograms
mg	milligrams
mg/L	milligrams per liter
min	minutes
mL	milliliters
mL/min	milliliters per minute

mm	millimeters
NRZ	naturally reduced zone
ppm	parts per million
PV	pore volume
RT	residence time
SI	saturation index
sorp	sorption
SOSWR	sum-of-squared weighted residuals
stagdiff	stagnant diffusion or exchange factor between mobile and immobile cells
stagpore	stagnant porosity or porosity of immobile cells
TOC	total organic carbon
TTP	Technical Task Plan
U	uranium
XRD	X-ray diffraction

Executive Summary

This project addresses the need to better understand the effects of slow uranium release rates on plume persistence and how these effects might influence groundwater remediation practices, including natural flushing. The main study questions are as follows:

1. How and where does uranium reside on the aquifer solids (i.e., uranium form and distribution)?
2. What are the uranium amounts and release rates from naturally aged aquifer solids?
3. What are the uranium release mechanisms?
4. How do the effects of questions 1–3 influence groundwater remediation strategies?

These questions are answered by characterizing the association between uranium contamination and associated minerals, conducting column experiments to determine rates of uranium release, developing a mechanistic reactive transport model of the release processes, calibrating the model using data from the flow-through column experiments, and using the model to help evaluate the potential effects of slow uranium release on water quality with natural versus enhanced flushing rates.

The adsorption of uranium on ferric oxyhydroxides commonly found in the shallow subsurface is well understood under controlled laboratory conditions. This is considered one of the main processes that can retain uranium on the solid phase, thus leading to slow uranium release and plume persistence issues. Numerous studies have addressed uptake and release of uranium by adsorption and desorption on minerals. However, field conditions are much more complex, including possible sorption on other mineral surfaces and delayed desorption due to diffusion in and out of less-mobile pore spaces (dual porosity).

This work focused on answering the study questions with detailed analyses of cores from 22 locations at the Grand Junction, Colorado, Site, which is managed by the U.S. Department of Energy Office of Legacy Management (LM). Although site-specific data are used, many other LM sites are also located in similar settings on alluvial floodplains, and it is likely that the information from this report can be applied to these other sites. Answering the study questions involved the use of selective chemical extractions (uranium amounts and where the uranium resides with depth), fission-track radiography with thin-section petrography (how and where does uranium reside on the microscopic scale), X-ray diffraction (uranium association with mineralogy), column testing (uranium release rates), and reactive transport modeling (uranium release mechanisms and influence on groundwater remediation strategies).

The selective extraction data indicate an increasingly effective removal of uranium with increasing aggressiveness of the leaching/digesting solution technique from carbonate leach to 5% nitric acid leach, to microwave digestion, to total digestion. It is likely that the 5% nitric acid leach removes the majority of uranium sorbed to mineral surfaces; however, definitive association of the uranium associated with each selective extraction versus the mineralogy cannot be interpreted without additional analyses.

The selective extraction data identify higher uranium concentration zones at the site that have secondary uranium deposited due to the uranium mill processes (1) above the water table

(most common), (2) below the water table in limited areas and likely associated with gypsum, and (3) near and below the water table in association with organic carbon.

Fission-track radiography indicates that uranium in the solid-phase samples is associated with (1) heavy mineral grains (i.e., monazites), (2) organic carbon, and (3) mineral coatings and cements that function as intragranular material, likely composed of iron oxyhydroxides and/or clays.

Column test data show an initial spike of uranium concentrations with the peak value related to the overall uranium content of the sample. After the peak concentration, uranium continues to be released, providing strong evidence for possible plume persistence issues in the field. Stopping the flow during the column tests indicated nonequilibrium conditions for uranium release within the columns, but the column flow velocities were much faster than field velocities. Most of the column tests only analyzed uranium in the column effluent water, but a larger column test was conducted with complete geochemical measurements. This column indicates the dissolution of gypsum based on the increase of calcium and sulfate concentrations in the column effluent water. The presence of gypsum was confirmed by the X-ray diffraction data. The data from this column were used for reactive transport modeling and an evaluation of geochemical processes.

Reactive transport modeling tested a variety of geochemical process models to provide information on which processes were most important. Sorption and dual porosity were the most important processes for calibrating modeled uranium data to measured column data. However, modeled sulfate and calcium concentrations are too low without the addition of gypsum. The modeling efforts showed a low sensitivity for dispersivity and some minor improvement with the addition of cation exchange. However, dispersivity may be an important parameter to include at the field scale.

Upscaling from the column tests to typical groundwater flow velocities was tested with the final calibrated reactive transport model. At the slower groundwater velocities similar to those in the field, the dual porosity (nonequilibrium) influences seen in the column test with higher velocity do not exist. Flow velocities are an important consideration when evaluating plume persistence under natural flow gradients and comparing possible remediation strategies. The use of groundwater tracer tests at the field scale is recommended for getting the best parameter estimates for reactive transport modeling, which can then provide a tool for testing possible remediation approaches before full implementation and provide significant cost savings.

Recommendations for evaluating plume persistence issues at a site are summarized as follows:

1. Make a thorough evaluation of existing mill-related uranium on the solid phase with depth.
2. Use microscopic techniques to determine where and how the uranium exists in the solid phase in association with the mineralogy.
3. Use tracer tests with companion column tests to determine contaminant release rates and mobility, which may include testing various influent fluids.

4. Calibrate reactive transport models using the data from recommendation 3 to get realistic input parameters (i.e., uranium sorption and dispersivity). This step should include the evaluation of parameter sensitivities and uncertainties.
5. Use reactive transport models with the final input parameters derived from recommendation 4 to evaluate flushing rates and test various remedial strategies. This step should include an evaluation of prediction uncertainties using sensitivity analyses.

To provide detailed guidance on the above steps and fill in current knowledge gaps, a follow-on technical task plan titled *Persistent Secondary Contaminant Sources* has already been developed.

This page intentionally left blank

1.0 Project Objectives

The objectives of this project are to determine uranium residence, amounts, and release rates from aquifer solids, better understand release mechanisms, and help estimate the effect of slow release rates on groundwater remediation methods. These goals are met by characterizing the association between uranium contamination and associated minerals, conducting column experiments to determine rates of uranium release, developing a mechanistic reactive transport model of the release processes, calibrating the model using flow-through column experiments, and using the model to help evaluate the effects of slow release on water quality.

This project addresses the need to better understand the effects of slow uranium release rates on groundwater remediation practices, including natural flushing. Although this study only examines contaminated sediments from the Grand Junction, Colorado, Site, the results provide a reasonable approximation of conditions that may affect many U.S. Department of Energy (DOE) Office of Legacy Management (LM) metal- and radionuclide-contaminated aquifers. No detailed studies are available that define uranium release rates from naturally aged contaminated sediments, similar to those at many LM sites.

The main study questions are as follows:

1. How and where does uranium reside on the aquifer solids (i.e., uranium form and distribution)?
2. What are the uranium amounts and release rates from naturally aged aquifer solids?
3. What are the uranium release mechanisms?
4. How do the effects of questions 1–3 influence groundwater remediation strategies?

Consistent with the Applied Studies and Technologies (AS&T) objectives, this project includes investigations of uranium release rates and residence times that will lead to better predictions of groundwater cleanup times (Table 1). Over the last 10–20 years, groundwater models were developed for many LM sites, providing a basis for comparing model predictions to current site conditions. Many of the models have not accurately predicted the concentrations of uranium over these time periods. In most cases, the models predicted more rapid cleanup than has actually occurred. Some studies suggest that rate-limited transfer of uranium from aquifer solids to groundwater may be a cause of this discrepancy. Thus, there is a need to understand rate-limited processes in order to develop more accurate predictions of groundwater cleanup rates. Many of the groundwater compliance decisions are based on predictions of the time frames for groundwater cleanup.

Table 1. Consistency of the Plume Persistence Project with the AS&T Objectives

AS&T Strategies Addressed	Specific AS&T Plume Persistence Tasks
1. Improve mechanistic understanding of essential physical, chemical, and biological processes	Uranium residence studies
	Release-rate studies
	Transport modeling
2. Evaluate the long-term performance of disposal cells, groundwater remediation approaches, and institutional controls	Improved capability for predicting uranium transport in groundwater
3. Evaluate and apply advances in science and technology to improve the sustainability of these remedies	Enhanced understanding of LM sites' groundwater

Actions being used or that have been considered to remediate groundwater or meet the compliance strategy at LM sites include (1) pump-and-treat (groundwater extraction and treatment), (2) surfactant flushing (injecting surfactants or complexing agents to enhance the mobilization and removal of contaminants), (3) natural flushing (allowing natural groundwater flow to flush the contaminants), and (4) gradient manipulation (using water-filled trenches or injection to enhance the natural gradient so that flushing occurs more rapidly). The focus of this study is a better understanding of the processes that may influence the effectiveness of a selected remedy. This understanding can then be used to improve the accuracy of model-based predictions for various remedial actions. Additional modeling of specific remedial strategies is beyond the scope of this report and will need to be completed on a site-by-site basis and/or with a follow-on technical task plan. Better predictive capabilities can promote faster acceptance of realistic cleanup times by stakeholders and regulators and ensure more effective management of LM sites.

2.0 Background and Study Approach

Initial surface contamination in the study area occurred due to tailings disposal from a pilot uranium mill ("large pilot plant") located at the Grand Junction site that operated from 1954 to 1958 (DOE 1989). The purpose of the large pilot plant was (1) amenability testing from a wide variety of commercial deposits to obtain metallurgical and cost data and (2) to develop and test new processes in pilot plants of sufficient size to permit accurate scale-up to commercial plants (McGinley 1987). Thus, the tailings from the large pilot plant were derived from various ores and processed using a variety of chemical reagents. Initially the tailings from the large pilot plant were discharged in a low area between the mill and a dike along the Gunnison River where they flowed downgradient and along the inside of the dike (McGinley 1987). Shortly after the large pilot plant startup (exact timing not established), a tailings slurry line was installed to fill an old gravel pit that was further north of the study area (McGinley 1987). Prior to remedial efforts, contamination was evaluated from radiological site characterization data conducted in 1985 (Henwood and Ridolfi 1986). The majority of the tailings at the site were removed by 1994 (DOE 2016). Remediation procedures are discussed in a DOE report (1995) where excavation depths were confirmed with subsoil testing for a radium standard below 5 picocuries per gram (pCi/g) in the surface (0–15 centimeter [cm]) and 15 pCi/g subsurface (below 15 cm) above background. Background for the site was 1 pCi/g radium-226.

At many LM sites, the former uranium mill tailings have been removed with excavations to depths based on radium standards. However, this does not guarantee the removal of secondary uranium sources that are not associated with the primary tailings. These secondary uranium sources are from mill-related or tailings fluids that are then sorbed, precipitated, or both on underlying native materials. As a result, even after several decades, high uranium concentrations in groundwater continue to persist and create "plume persistence" issues. The Grand Junction, Colorado, Site provides a convenient location for testing the mechanisms that create continued release of uranium from the solid phase into the water phase from these secondary sources. This report is a summary of the work on the plume persistence project relating to the Grand Junction site with the goal of transferring the findings from this site to other LM sites. The Grand Junction site was selected for study under the plume persistence project partially due to its location next to the Grand Junction office, which allows for quick and easy access.

A first step in understanding the mechanisms of uranium release is to determine the minerals with which the uranium is associated (mineral residences). Determining mineral residences in fine-grained materials is not straightforward and typically requires an interpretation of data from multiple laboratory techniques, as discussed in Sections 3.0 and 4.0. Accurate prediction of uranium release rates from aged aquifers needs to consider multiple geochemical processes, including the kinetics of the solid-to-groundwater transfer, which is evaluated through column testing (Sections 3.5 and 4.2). These processes are considered individually and in combination as part of the mechanistic reactive transport modeling (Sections 3.6 and 4.4). The final reactive transport model is then used to evaluate uranium release rates from a simulated column test with influent flow velocities that are more typical of groundwater flow rates (Section 4.4).

2.1 Uptake and Release of Uranium

Uranium exists in nature in both oxidized and reduced forms. Oxidized species are more likely to be present than reduced species in the shallow alluvial aquifers found at many LM sites. However, localized reduced zones without oxygen can also affect transport. Strong reducing potentials can cause uranium to precipitate as minerals, such as uraninite. Oxidation promotes uranium mobility; however, with highly elevated concentrations of some solution species, precipitation is possible (e.g., precipitation of uranyl carbonates or uranyl vanadates). Available thermodynamic data can be used to predict the stability of the majority of minerals that are likely to form. Uranium transfer between solids and groundwater in the shallow alluvial aquifers under consideration is probably governed primarily by adsorption reactions; uranium transfer that is due to precipitation and dissolution is likely to be relatively minor in oxidized portions of these aquifers. However, mineral precipitation or dissolution could be purposely promoted for groundwater remediation.

At many LM sites, the underlying groundwater was influenced by leachates from industrial processes (such as ore milling) that liberated silica, iron, alumina, sulfate, and carbonate. Thus, minerals consisting of these major components may have precipitated in the aquifer. Uranium could have been incorporated into these minerals, or contaminated surfaces could have been shielded by the precipitation of mineral overgrowths. The subsequent release of uranium would then be governed by the dissolution of these armoring phases. The thermodynamic stabilities of many of these major mineral phases (e.g., calcite, siderite, gypsum, quartz) are well established; however, the stability fields for others, including amorphous materials such as iron oxyhydroxides, are less precise. Predictions of uranium release using thermodynamic stability

data and assumed equilibrium will be accurate only if the mineral coatings dissolve rapidly (minutes to days, depending on the remediation scheme being considered). Some carbonate and sulfate minerals will dissolve in these time frames, but many silicates and other minerals will not. For slow-dissolving minerals, uranium release is determined by dissolution rates rather than thermodynamic equilibrium.

Numerous studies have addressed the uptake and release of uranium by adsorption and desorption on minerals. The adsorption of uranium and metals on ferric oxides and oxyhydroxides common in the shallow subsurface is well understood under laboratory conditions (e.g., Davis and Leckie 1978; Tripathi 1984; Hsi and Langmuir 1985; Morrison et al. 1995; Davis et al. 2004). Adsorption of uranium to these ferric oxides is the result of inner-sphere chemical bonding to specific surface-complexation sites (Davis and Leckie 1978; Dzombak and Morel 1990). Complexation theory involving both aqueous complexes and surface-bound complexes is capable of accurately predicting these adsorption processes at equilibrium. Dzombak and Morel (1990) summarize the available adsorption data for uranium on amorphous ferric oxyhydroxide (AFO) and present a site complexation model that is consistent with the data available at that time. Ames et al. (1983) provide data for the sorption of uranium to clays and amorphous silica. Equilibrium sorption studies also exist for manganese oxides, quartz, and other mineral phases common to shallow aquifers.

Mineral adsorption sites may be in contact with the bulk groundwater or separated from it by immobile groundwater through which the contaminant must diffuse. For example, a shale bed can contain immobile water in disconnected pores, a phenomenon which is referred to as dual porosity. Contaminants may diffuse into this immobile pore fluid and become isolated from advection. The contaminants may subsequently adsorb on mineral surfaces within the pores. Release of this isolated contaminant will be limited by outward diffusion rates.

2.2 Methodology to Determine Uranium Residences

Each mineral phase has a unique and often predictable way in which it reacts with uranium. Thus, prediction of the release of uranium from aquifer solids is enhanced by information about the minerals with which the uranium resides. Numerous techniques are available to help determine these associations between minerals and contaminants. Unique techniques for this study include selective chemical extraction and fission-track radiography, in addition to traditional thin-section petrography and X-ray diffraction (XRD). The uranium in the targeted samples is likely to be associated with very fine-grained material. Determination of the uranium residence in fine-grained materials is complicated because rarely can individual phases be separated from the bulk matrix.

Because uranium is the only fissionable element in the samples that produces observable tracks, fission tracks are a direct indicator of uranium. A sufficient neutron flux is required for uranium to fission. The neutron flux is applied by placing the samples in a nuclear reactor for a period of about 2–8 hours (h). Because uranium is a key contaminant at many LM sites, fission-track analysis provides a unique opportunity to obtain detailed, low-cost information about contaminant residence. Ledger et al. (1984) used fission-track maps to determine the residences (e.g., point sources, fracture linings, or grain coatings) of uranium in 50 igneous rocks. Zielinski et al. (2007) used fission tracking to determine the residence of uranium in sediments near historical mining districts.

Selective chemical extractions use a chemical solvent to partially dissolve a solid sample. Ideally, the solvent will dissolve only one mineral phase. Thus, the amount of contaminant removed by the solvent is a quantitative measure of the amount contained in that specific mineral phase. Selective chemical extractions have been developed for a variety of minerals in geologic materials, including ferric and manganese oxides, humic organic matter, allophane (amorphous silica alumina compounds), and carbonate minerals. Smith and Mitchell (1987) provide a summary of selective chemical extraction techniques. Unfortunately, several problems often accompany selective chemical extractions because ideal solvents do not exist. Even though some solvents appear to be reasonably specific, they often dissolve more than one phase. Because some solvents rely on slow dissolution kinetics, agitation time is important. An example is the commonly used ammonium oxalate extraction of amorphous ferric oxyhydroxide that also extracts allophane (Smith and Mitchell 1987) and magnetite (Schwertmann and Cornell 1991). Correlations of the concentrations of oxyhydroxide phases with uranium concentrations can be useful in determining whether the oxyhydroxide phases are important residences for uranium.

2.3 Methodology to Determine Uranium Release Rates

Column studies were completed to determine uranium release rates from collected core samples. These columns were filled with dry sediment and filled with an influent solution from the bottom up to reduce air bubble entrapment, and the effluent was then sampled at consistent intervals. The influent solution was prepared in the laboratory with the dissolution of stock solids to produce water that had a geochemistry equivalent to that of the nearby groundwater, thus, creating conditions that are similar to those of groundwater inflow. Eleven core samples with the greatest concentrations of uranium and two samples with the smallest concentrations of uranium were chosen for column testing. Eleven smaller columns (one column for each core sample) allowed for the determination of uranium concentrations in the effluent water with time, which was then converted to pore volumes. Filling the column one time is equivalent to one pore volume. Results from the eleven columns are compared in this report for maximum uranium release and subsequent release rates through time, which is normalized by the use of pore volumes.

One larger column was completed to allow for a larger sample volume, which was analyzed for a complete set of major cations and anions and several other metals, as well. These column data were then used in the reactive transport modeling. In addition, the flow in all of the columns was temporarily halted at 25 and 50 pore volumes for 24 hours and 4 days, respectively, in order to test whether or not the column water was in equilibrium with the solid phase. This is referred to as stop-flow testing.

2.4 Reactive Transport Modeling

Reactive transport modeling goes beyond traditional contaminant transport modeling by including mineral reactions, such as sorption and mineral dissolution/precipitation that can occur along the flow path. Geochemical modeling programs, such as PHREEQC (Parkhurst and Appelo 2013), can account for these geochemical changes, and PHREEQC is well suited for one-dimensional (1D) simulations of column tests. Geochemical modeling often assumes equilibrium, but the slow release of uranium that may be due to rate-limited mechanisms can be included.

Slow release rates may control uranium release from contaminated alluvial aquifer sediment on time scales of hours to months. The slow release could be due to rate-limiting, surface-complexation reactions, incorporation into the atomic lattice, or diffusion out of the interior of a particle followed by rapid-equilibrium and surface-complexation reactions. Other chemical processes—including many aqueous-complexation, mineral-precipitation, and mineral-dissolution reactions—proceed fast enough to be considered at equilibrium. Thus, predictive models may need to consider both equilibrium and kinetic chemical reactions.

Modeling of sorption and desorption of metals to many oxyhydroxide and clay minerals is well advanced for systems at equilibrium. For example, modeling using site complexation theory has been successful in predicting the adsorption of various trace metals to synthetic AFO (e.g., Dzombak and Morel 1990). Equilibrium concentrations are readily calculated by computer codes that simultaneously solve the set of mass action expressions, mass balance expressions, a proton condition, and an electron condition for the system. Evaluation of remediation practices requires a flow-and-transport model that considers the slow kinetics of chemical transfer from solids to groundwater. PHREEQC incorporates this transfer as a dual porosity approach with mobile and immobile cells along with a mass transfer coefficient.

2.5 Data Needs

The initial data were obtained from core samples collected at the Grand Junction site (22 core holes, see Figure 1 and Section 3.1) and studied using flow-through column tests (see Section 3.5). The cores were characterized for mineralogy (such as calcite, gypsum, and metal oxyhydroxides) and uranium residence (amounts and location, small and larger scale). Petrography, fission tracking, and selective extractions were used to determine the uranium distribution in the collected cores, along with identification of uranium residence at the pore scale. Uranium extractions (see Section 3.2) were performed at the Environmental Sciences Laboratory (ESL) in Grand Junction, Colorado, and ESL microscopes were used for petrography and fission tracking (see Section 3.3). Column tests (see Section 3.5) were used to better quantify the uranium release rates and amounts and were also completed at the ESL. One column with all the necessary parameters for input into a 1D reactive transport model was also completed (see Section 3.6 for modeling procedures). The above data needs are paired with specific project questions in Table 2 discussed in the next section.

2.6 Variables Summary

Key variables are uranium form and distribution on the aquifer solids, uranium concentrations and release rates from column tests, and the transport parameters associated with each release mechanism (Table 2). The transport parameters for release mechanisms listed in Table 2 were estimated during the model calibration and included the following variables: water-phase geochemistry, solid-phase geochemistry, sorption equilibrium constants, sorption site densities, column porosity, dual porosity diffusion rates, mineral equilibrium constants, mineral dissolution/precipitation kinetic rates, and cation exchange capacity. The calibration process assists in determining which release mechanisms are occurring and which mechanisms are most important in reproducing the measured data.

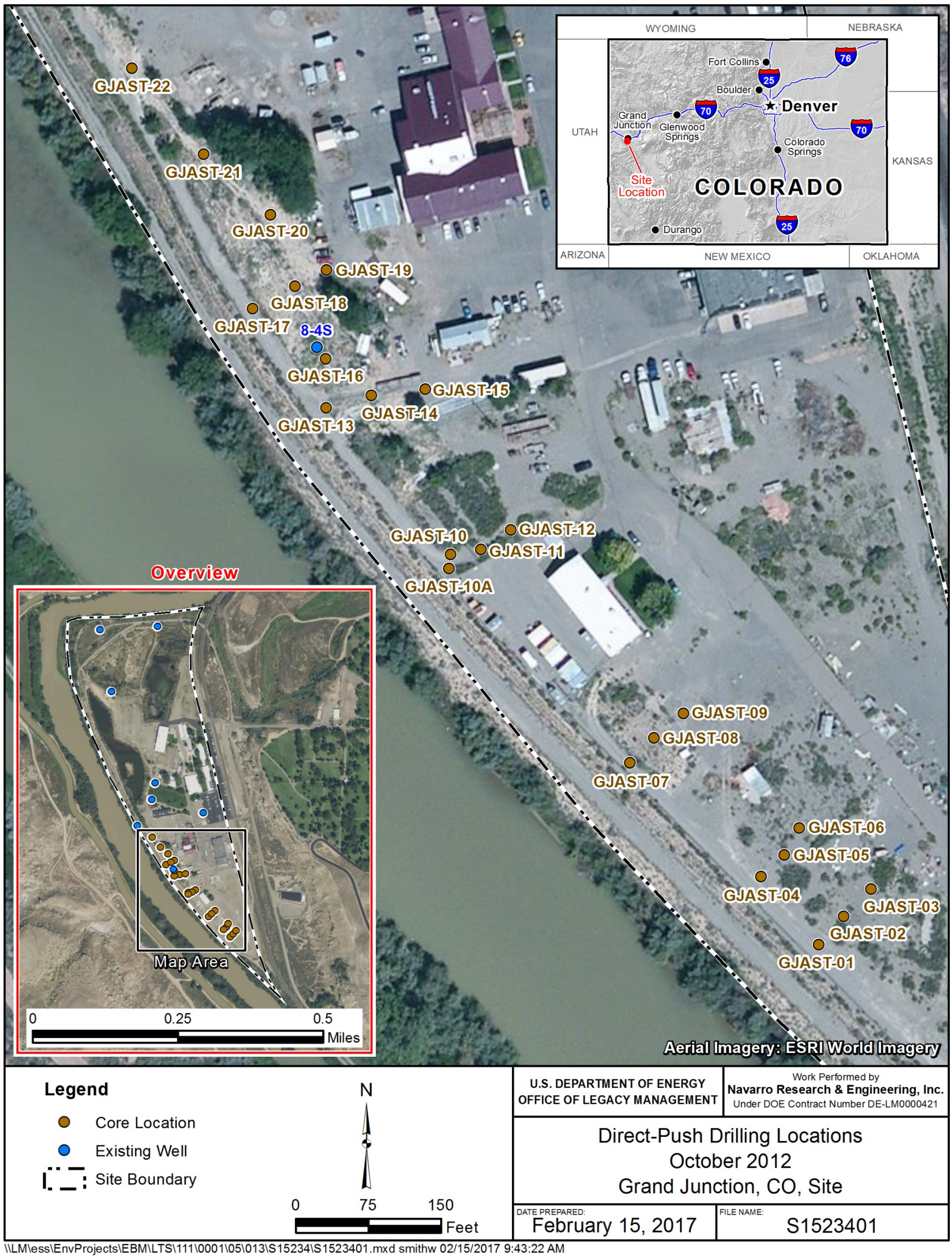

Figure 1. Grand Junction Site Core Locations

This page intentionally left blank

Table 2. Plume Persistence Study Questions with Related Data Needs, Variables, and Data Analysis

Question	Data Needs	Variables	Data Analysis	Comments
How and where does uranium reside on the aquifer solids?	Core samples	Uranium form and distribution determined from petrography, fission tracking, and selective extractions	Evaluation of uranium distribution at the field scale (using three-dimensional visualization) and the pore scale	
What are the uranium amounts and release rates from naturally aged aquifer solids?	Column tests	Uranium concentrations and release rates	Uranium concentrations through time will be used as calibration data for reactive transport modeling	Full geochemistry suite is needed for reactive transport modeling
What are the contaminant release mechanisms?	Column tests	Uranium transport parameters associated with each release mechanism (sorption, dual porosity, mineral precipitation and dissolution, and cation exchange)	Parameter sensitivities from model calibration will help determine which mechanisms are most important	
How do the effects of the above questions influence groundwater remediation strategies?	Calibrated mechanistic numerical model	Different remedial strategies (i.e., natural flushing, pump and treat, etc.)	Different remedial strategies will be evaluated for effectiveness using the calibrated model	Preliminary work completed for this report, with additional work to be completed as part of a follow-on Technical Task Plan

3.0 Methods

This section describes the collection of the soil samples used in the column tests, the selective extraction methods, the methods used for the column study, and methods for XRD, petrography, and fission-track radiography. A complete description of the selective extraction and analytical methods can be found in the *Environmental Sciences Laboratory Procedures Manual* (LMS/PRO/S04343) (http://sp.lm.doe.gov/Contractor/ControlledDocuments/Controlled Documents/S04343_ESL Procedures.pdf). When applicable, the method numbers in this ESL procedures manual are indicated in the following methods sections.

3.1 Sample Collection and Preparation

All soil cores (Figure 1 and Table 3) were collected from the shallow alluvial aquifer at the Grand Junction site with a direct-push drilling rig in areas that have had historically high groundwater uranium concentrations. The general study area was selected based on high concentrations of radium contamination in the shallow (up to 10 feet [ft]) sediment that was related to tailings disposal. The former tailings were removed in 1994. Composite core samples were collected from each 1 foot of core from the ground surface to the underlying bedrock, or refusal, for a total of 360 samples. The samples were collected from river alluvium consisting mostly of silt, sand, gravel, and clay and then composited over each foot of unconsolidated drill core, air-dried, and sieved to less than 2 millimeters (mm) diameter per ESL procedures before additional solid-phase testing.

Table 3. Grand Junction Site Borehole Summary

Borehole	Date	Northing	Easting	Depth to Bedrock (ft)	Refusal Depth (ft)	Total Depth (ft)	Ground Surface Elevation (ft)
GJAST-01	10/15/12	454043.481	1127944.668	23.5		25.0	4570.25
GJAST-02	10/15/12	454072.875	1127970.43	24.0		24.5	4569.69
GJAST-03	10/15/12	454101.112	1127998.864	24.8		25.0	4570.49
GJAST-04	10/16/12	454113.638	1127885.238		7.0	7.0	4570.18
GJAST-05	10/16/12	454136.164	1127909.121		22.5	22.5	4570.21
GJAST-06	10/16/12	454163.967	1127924.412		20.0	20.0	4570.29
GJAST-07	10/16/12	454231.191	1127749.836	24.7		25.0	4569.78
GJAST-08	10/17/12	454256.882	1127774.36	24.0		25.0	4570.41
GJAST-09	10/17/12	454282.388	1127804.871		6.5	6.5	4570.67
GJAST-10A	10/17/12	454432.03	1127562.654		4.0	4.0	4568.91
GJAST-10	10/23/12	454446.57	1127564.717	22.0		25.0	4568.53
GJAST-11	10/17/12	454451.432	1127595.63	20.5		25.0	4568.64
GJAST-12	10/18/12	454471.847	1127626.854			20.0	4568.71
GJAST-13	10/18/12	454597.678	1127436.075	23.5		24.5	4568.33
GJAST-14	10/18/12	454610.346	1127482.642	21.7		24.7	4568.48
GJAST-15	10/18/12	454616.852	1127538.472	20.5		24.0	4568.92
GJAST-16	10/18/12	454648.306	1127435.659	21.0		25.0	4567.70
GJAST-17	10/22/12	454700.052	1127359.993	24.0		24.5	4568.26
GJAST-18	10/22/12	454723.124	1127403.937	21.7		25.0	4567.72
GJAST-19	10/22/12	454740.018	1127436.549	21.8		22.3	4568.28
GJAST-20	10/22/12	454797.194	1127378.501	20.7		21.0	4568.16
GJAST-21	10/23/12	454859.668	1127309.424	21.2	21.5	21.5	4567.70
GJAST-22	10/23/12	454948.11	1127235.409	22.5		23.0	4567.84

Note:
Datum is NAD27.

3.2 Selective Extraction

Separate split samples of all sediment core samples were extracted using five different methods with the respective ESL manual method number in parentheses; carbonate extractions (SE(CARB-1)), 5% nitric acid extractions (CB(BT-1)), microwave digestions (SE(MD-1)), total digestions by lithium metaborate ($LiBO_2$) fusion using a platinum crucible (SE(TD-1)), and ammonium oxalate extractions (SE(AO-1)). With all of these techniques, uranium concentration in the liquid phase created by each extraction or digestion is measured but is also reported as the mass of uranium relative to the mass of the initial solid-phase sample.

Each of the selective extraction methods is designed to extract different forms of uranium from the soil cores. For example, the carbonate extraction, the 5% nitric acid extraction, and the microwave digestion are designed to extract labile uranium or uranium adsorbed to soil particles. The total digestion is designed to dissolve mineral grains and, thus, should extract all of the uranium and other trace elements in a sample, adsorbed as well as that present in the mineral

grains of a sample. The ammonium oxalate extraction is designed to remove all noncrystalline iron in a sample, thus dissolving any iron oxyhydroxide coatings or cements. The 5% nitric acid extraction has been used frequently by DOE in previous studies (Morrison 2016), but the relative extraction efficiency of the carbonate extraction, 5% nitric acid extraction, or microwave digestion is unknown. The relative extraction efficiency of all the selective extraction methods is discussed further in the results section (see Section 4.1).

Dissolved uranium was analyzed with laser-induced kinetic phosphorescence analysis. Some extraction samples were also analyzed for Fe, Mo, or Mn using inductively coupled plasma-optical emission spectroscopy (methods AP(Fe-5), AP(Mo-5) and AP(Mn-2), respectively).

3.3 Petrography and Fission-Track Radiography

Fission-track radiography was done in combination with petrography to determine the association of uranium with aquifer sediments. Uranium concentrations in the solid phase at LM sites are commonly too low to be positively identified, even using electron beam techniques. With these low uranium concentrations, determining what mineral grains the uranium is associated with is very difficult to ascertain via more traditional techniques. However, deductions about mineralogy from petrographic methods and associated uranium from fission-track radiography are often possible. Petrography was completed using plain light, oblique light, reflected light, and crossed Nicol prisms. The petrography focused more on the identification of mineral coatings and cements than on detailed mineral identification, since this project is looking at secondary uranium associated with coatings and cements and not primary uranium associated with the mineral grains.

Fission-track radiography involves the irradiation of a uranium-bearing sample with a flux of thermal neutrons that causes induced fission of the highly fissionable uranium-235 isotope. Fission fragments recoiling from the sample surface can be detected by covering a polished thin section with a suitable detector material. This detector material is typically muscovite mica or Lexan plastic. Fission fragments entering the detector cause structural disturbances that can be developed for optical inspection by subsequent etching of the detector with concentrated hydrofluoric acid (for mica) or sodium hydroxide (for Lexan). For this study, fission-track detectors using mica and Lexan were tested, but the mica detector was superior from the Lexan detector. Thus, only the results from the mica detector are presented in this report. The developed fission tracks observed under a microscope reveal sources of uranium in the thin section much as autoradiographs but with much greater sensitivity and resolution. Thorium is a possible source of fission fragments, but its sensitivity to thermal neutron fission is approximately 100 times less than that of an equal concentration of uranium. Highly fissionable plutonium can also be mapped by this method.

Slides were prepared by polishing a thin section of an epoxy-impregnated sample of interest and modified by grinding to fit in containers for irradiation. Polished thin sections are preferred because they permit the most intimate planar contact between the thin section surface and the detector (mica or Lexan). Poor contact during irradiation will produce poorer spatial resolution of uranium sites and a fuzzy image of fission tracks.

The mounting of the mica detector requires obtaining relatively pure muscovite mica from sheet stock. The mica was checked for low uranium content by irradiating a thin sheet of it under

typical irradiation conditions, etching it (see below), and checking for the presence of induced fission tracks. Thick books of mica sheets were progressively thinned and separated by inserting a razor knife along an edge and twisting. These actions expose fresh cleavage faces to be inspected for clarity, uniformity of surface, and freedom from scratches. The thickness of the final mica sheet used for a detector is not critical but should be sufficient to avoid curling, allow easy handling, and permit clear distinction of upper and lower surfaces under the microscope. A final freshly exposed planar surface (cleavage face) of the chosen mica detector was obtained by applying a complete covering of Scotch tape that also contacts the mica edges and then peeling it off. This freshly exposed surface was again inspected for freedom from scratches or other obvious defects. The chosen sample of mica was further trimmed with scissors to the proper rectangular size, applied fresh-face down on the thin section, and affixed with a covering of Scotch tape. Prior to mounting, one corner of the rectangular mica was cut to aid in later determinations of original mica-slide orientation. Further aids to orientation included a series of holes manually bored through the mica and ending on the slide surface. Typically, three holes are bored along one short edge of the mounted mica and two holes are bored along the opposite edge that has one corner missing.

The prepared thin section slides were placed in polyethylene tubes and irradiated in a research reactor at the U.S. Geological Survey in Denver, Colorado. These tubes are cylindrical and will accommodate a vertically oriented thin section, but only after grinding ~1–2 mm off the long dimension of the original thin section. The thin section was placed into the polyethylene tubes with a polyethylene foam "back-a-rod" of 1-inch diameter that is partially slit lengthwise to enclose the thin section and mica. This foam enclosure places some pressure on the thin section to provide good contact of mica and thin section surface during irradiation. Samples were irradiated at a neutron flux of 2×10^{12} neutrons per square centimeter per second for 8 hours for a total maximum neutron dose of $\sim 11.6 \times 10^{16}$ neutrons. Irradiated samples are allowed to decay in storage for about 6 weeks or more after irradiation to allow for the decay of some shorter-lived neutron activation products.

After irradiation, the muscovite mica detector is removed from the recovered thin section with a razor knife that is carefully inserted underneath the mica and slid along and around the borders of the mica to cut any Scotch tape. The mica detector and the adherent Scotch tape on its upper surface are immersed in reagent-grade hydrofluoric acid for 10 minutes in a Teflon crucible. After about 5 minutes, the Scotch tape can easily be peeled off the mica with tweezers and removed. After 10 minutes, the mica is removed and transferred to a large plastic beaker containing water. The mica is washed with a strong stream of water and then alcohol and set to dry overnight. The dried mica was mounted on a fresh glass slide using minimal amounts of Scotch tape placed along the ends. The mica was mounted original side down, in the same orientation as during irradiation, as indicated by comparison to the paired original thin section.

The distribution of uranium in the original thin section is indicated by the distribution of fission tracks in the mica detector, observed under the microscope. The focus of the microscope is adjusted to view the underside of the mounted mica that was the surface in contact with the thin section. Etched fission tracks appear as linear features approximately 5 microns long and are observed under various magnifications. Using spatial relationships between features of the fission-track image, the bored reference holes in the mica, corresponding areas of bored damage on the thin section surface, a mechanical stage, and a gridded eyepiece, one can locate areas of interest on the mica fission-track detector and find the same location on the original thin section. Paired areas of fission tracks and thin section were photographed for documentation. Once

identified, areas of relatively high fission-track density (and therefore relatively high uranium concentration) can be revisited and further characterized in the original thin section using electron microprobe or scanning electron microscope. Note that the detection limit for uranium by scanning electron microscopy is on the order of several hundred to one thousand parts per million (ppm), so the greater sensitivity of the fission-track technique provides distinct insights for many samples of low-to-moderate uranium concentrations.

3.4 X-Ray Diffraction

XRD for mineralogic analysis was completed on one sample by William Hood in the XRD laboratory at the Colorado Mesa University in Grand Junction, Colorado. The sample was ground for 10 minutes in a micromill to reduce the particle size to about 40 microns or less. Diffraction analyses were done using a Rigaku Miniflex X-ray diffractometer run at 35 kilovolts and 15 milliamps. All scans were conducted from 3 to 50 degrees 2-theta at 2 degrees per minute. A Rigaku software program was used to calculate the diffraction peak positions and area under the curve for the various peaks. This procedure provides relative mineral abundances but cannot be consider truly quantitative because the Rigaku algorithm cannot fit every peak exactly.

3.5 Column Testing

Eleven core samples with the greatest concentrations of uranium and two core samples with the smallest concentrations of uranium were chosen for column testing. These are the same samples used for thin sectioning and fission-track radiography. Air-dried core samples that were sieved to less than 2 mm were used to fill a column with a total volume of 20.85 milliliters (mL). Care was taken to obtain a representative sample by mixing the sample and minimizing particle size/density bias. Sediment was placed in each column in approximately 1 cm lifts with gentle tapping between lifts.

Each column was leached with laboratory-prepared water that matched the composition of groundwater collected from well 8-4S on December 14, 1999, as close as possible. The laboratory water was prepared by dissolving the amount of minerals listed in Table 4 in 1 liter (L) of solution to produce the final water listed in Table 5. The final solution pH was adjusted to 7.0 using nitric acid, which resulted in an alkalinity as $CaCO_3$ of 300 milligrams per liter (mg/L). As additional columns were completed, new influent solution was prepared and measured to confirm final preparation within 5% of the target concentrations. A Masterflex peristaltic pump with number 13 nylon tubing was used to pump synthetic well 8-4S water through the column from bottom to top (Figure 2). The synthetic well 8-4S water was kept in a collapsible plastic container to minimize exposure to air. The columns were run at a rate of approximately 0.10 milliliters per minute (mL/min) for a residence time of about 1 hour per 1 pore volume. After 25 pore volumes, the flow was stopped for 24 hours. The columns were then run for 25 more pore volumes, and flow was stopped for 4 days. The columns were then run for an additional 25 pore volumes. Because of occasional plugging issues, the full number of pore volumes was not reached for every column. Each test took approximately 8 days. Samples were collected every 100 minutes (~10 mL) and analyzed for uranium.

Table 4. Amount and Selected Solid Phase for Column Influent Solution

Solid Phase	Amount Added (mg/L of solution)
$NaHCO_3$	575.0
Na_2SO_4 (anhydrous)	440.0
$CaSO_4 \cdot 2H_2O$	847.5
$MgSO_4 \cdot 7H_2O$	320.0
K_2SO_4	19.0
$MgCl_2 \cdot 6H_2O$	250.0

Table 5. Target Concentrations for Column Influent Solution

Analyte	Target Concentration
pH	7.0
Alkalinity as $CaCO_3$ (mg/L)	300
Sodium (mg/L)	300.0
Potassium (mg/L)	8.530
Magnesium (mg/L)	61.45
Calcium (mg/L)	197.4
Sulfate (mg/L)	905.5
Chloride (mg/L)	87.31
Uranium (µg/L)	0.0

Abbreviation: µg/L= micrograms per liter

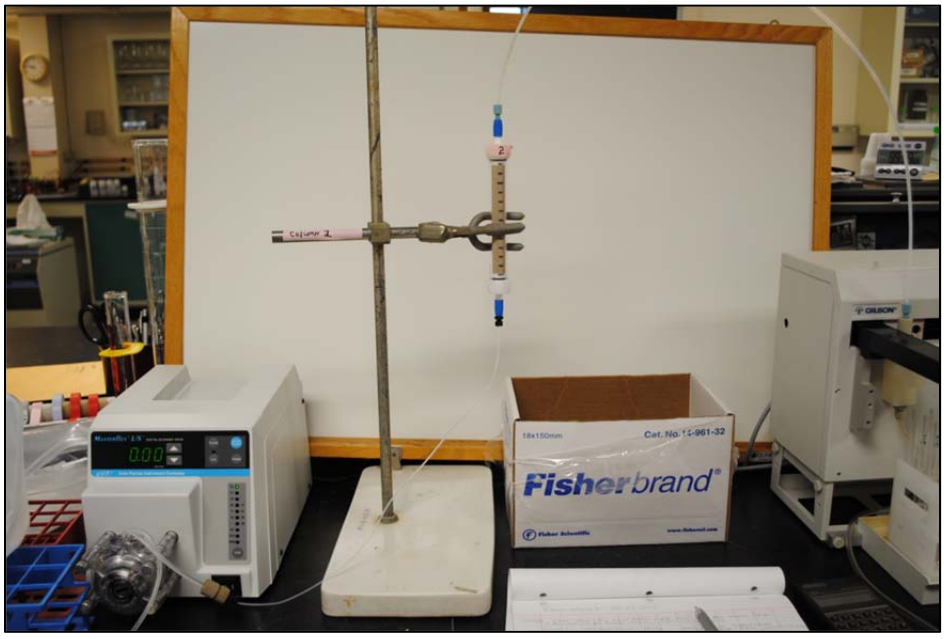

Figure 2. Column Testing Setup (flow is upward)

The pore volume (PV) was determined by multiplying the flow rate by the length of time required to fill the column with synthetic well 8-4S water. A fraction collector was used to collect column effluent in glass test tubes. The flow rate was set on the pump but was accurately determined from the volume collected during each collection period. Residence time (RT) was calculated as follows:

$$RT = (PV/60)/AFR$$

where

RT = residence time in h
PV = pore volume in mL
AFR = average flow rate in mL/min

One core sample, GJ 20-10, was chosen to fill a larger column that was 21.3 cm long × 2.5 cm wide for a total volume of 104.6 mL. Except for a target flow rate of 0.15 mL/min and sampling every 170 minutes instead of 100 minutes, the same procedures used for the smaller columns were utilized. The stop-flow event at 25 pore volumes was 62.8 hours, and the stop-flow event at 50 pore volumes was 10 days. The main purpose of the larger column was the larger water volume, which allowed for analyses of all major cations and anions and iron, uranium, and total organic carbon, as well. These data were then used for one-dimensional reactive transport modeling.

3.6 Reactive Transport Modeling

The larger column test data was analyzed using the geochemical modeling program PHREEQC (Parkhurst and Appelo 2013) using a 1D reactive transport model. PHREEQC modeling used a 1D column with 20 cells for a cell length of 0.01065 m and the influent water chemistry of the synthetic well 8-4S water (Table 5). The column was run continuously without any equilibration time, so the simulations with PHREEQC used the analytical results from the first effluent water sample collected at 0.83 PV (Table 6) to simulate initial conditions. PHREEQC provides for an initial equilibration of the water phase with the solid phase. In PHREEQC, this equilibration is necessary for simulating uranium sorption and cation exchange. This equilibration adds the initial modeled amount of uranium sorbed onto the solid phase based on the sorption parameters and the uranium in the initial water. Likewise, the full complement of cations is added onto the solid phase for subsequent cation exchange, based on the initial solution geochemistry (0.83 PV in this case).

A sequential order of processes was simulated to avoid adding too much complexity in one step. Initial calibration was done manually to provide a better understanding of the different processes before proceeding to automated calibration. Only the final automated calibration results are presented in this report. Processes of sorption, dual porosity, mineral dissolution, dispersion, and cation exchange were evaluated separately and in combination. Sorption was simulated using the generic surface complexation model of Davis et al. (2004) with calibration proceeding through the use of varying sorption equilibrium constants and surface site densities. Dual porosity was simulated using a single exchange factor between mobile and immobile cells, which is part of the 1D transport code in PHREEQC. The PHREEQC database was updated to use the ternary complexes of uranyl and carbonate with alkaline-earth metals (Mg^{2+}, Ca^{2+}, Sr^{2+}, and Ba^{2+}) from Dong and Brooks (2006) and new uranium thermodynamic data from Guillaumont et al. (2003).

Final calibration for all parameters used the inverse modeling techniques (automated calibration) of PEST (Doherty 2005) for every analyzed pore volume and all measured analytes.

Table 6. Chemistry of a Few Select Analytes for the Column Influent Water and the First Water Sample That Was Used for Assumed Column Equilibration in the Reactive Transport Model

Analyte	Influent Water	Equilibration Water at 0.83 PV
pH	7.0	7.6
Alkalinity as $CaCO_3$ (mg/L)	313	101
Calcium (mg/L)	192	530
Sulfate (mg/L)	918	4180
Uranium (µg/L)	0.0	2000

Abbreviation:
µg/L= micrograms per liter

3.7 SLAC Support

Researchers from the SLAC National Accelerator Laboratory (operated by Stanford University and funded by the U.S. Department of Energy Office of Science) have ongoing research on naturally reduced zones (NRZs). Much of their research has focused on LM's Old Rifle, Colorado, Site in the past, but current research has expanded to the upper Colorado River basin, including other LM sites along river flood plain areas, such as the Grand Junction site.

SLAC was supported under the plume persistence project by collaboration with LM's prime contractor, Navarro Research and Engineering, Inc. This support was provided by the contractor operating a direct-push drilling machine for the collection of cores as several LM sites. The SLAC focus was the collection of NRZ material during several core collection efforts, mainly in 2014. All analyses on those cores were completed by SLAC, and that work will be reported by them in separated publications and is not a part of this report. This work will contribute valuable information to ongoing plume persistence work and to LM's general understanding of natural flushing stagnation, as NRZs are potential repositories for uranium but also can provide long-term uranium release. Ongoing work by SLAC is anticipated and is part of the follow-on *Persistent Secondary Contaminant Sources* Technical Task Plan (TTP). Future reactive transport modeling may use information on NRZs for better predictions of overall uranium mobility and potential plume stagnation.

4.0 Results and Interpretations

Prior to remedial efforts, contamination was evaluated from radiological site characterization data conducted in 1985 (Henwood and Ridolfi 1986). For reference, these data are provided for the study area (Figure 3) with the highest radium-226 values detected at each measured location in comparison with the drilling locations. In addition, the original estimates of contamination depths before remediation were evaluated by a DOE report (1989), and these depths are provided in Figure 4, along with borings GJAST-01 through GJAST-22. The radium-226 values and estimated depths of contamination provide a general guide for where the former tailings were located in this area (Figure 3 and Figure 4, respectively).

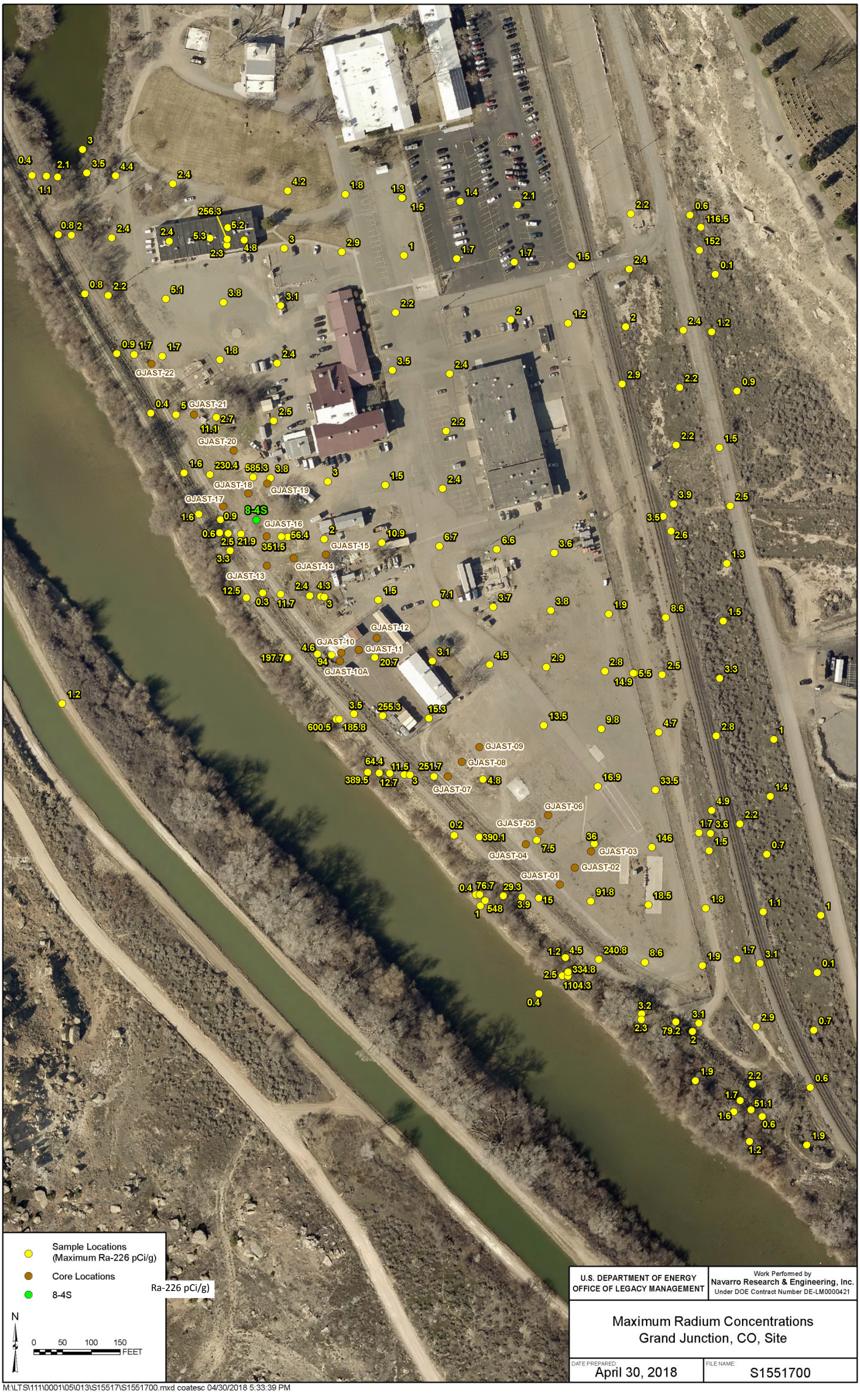

Figure 3. Highest Measured Radium-226 Values at Each Measured Location from Henwood and Ridolfi (1986) in the Study Area

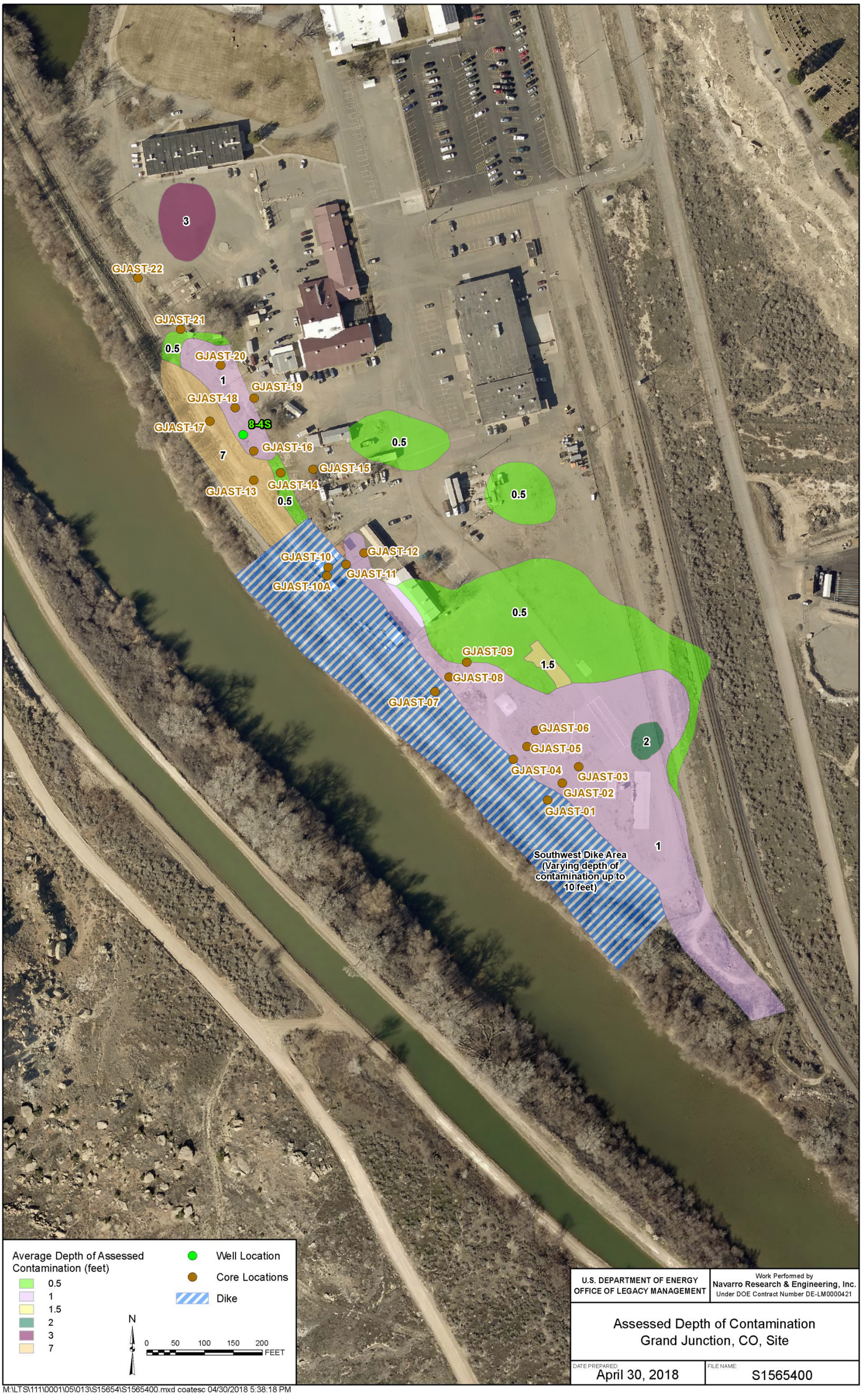

Figure 4. Estimated Contamination Depths from DOE (1995) in the Study Area

Boring logs for all 22 direct-push drilling locations (GJAST-01 through GJAST-22) can be found in Appendix A. These logs indicate typical river floodplain alluvium with mainly sand and gravel with occasional silt layers. Depth to bedrock (Morrison Formation) is 20–25 ft (Appendix A and Table 3). Final excavation depths were reported in the *Final Report of the Decontamination and Decommissioning of the Exterior Land Areas at the Grand Junction Projects Office Facility* (DOE 1995) based on the average of specific areas. These average depths were evaluated for each borehole location (GJAST-01 through GJAST-22) and ranged from 12 to 60 inches to a maximum of 82 inches. However, the final amount of backfill material could not be determined from previous reports, as there was no report on the final regrading of the area to ground surface elevations. The boring logs attempted to indicate the depth of backfill material, but it is likely that the backfill material was also alluvial river floodplain sand and gravel, thus making backfill very difficult to distinguish from native floodplain material.

Data for each soil sample with loss on drying and the mass passing the 2 mm size fraction are provided in Appendix B (Tables B1 and B2, respectively). These data are not used directly in this report but may be useful for future work and are reported in Appendix B for completeness. In general, the <2 mm size fraction data and higher values of loss on drying are indicative of zones with finer-grained sediments.

XRD analyses were completed only on sample GJAST-20-10. The results for relative abundances of minerals are 63% for quartz, 23% for feldspar, 7% for calcite, 3% for gypsum, 3% for clay, and a trace of mica, all by weight percent. These values are qualitative and are used in this report only for XRD confirmation of the presence of calcite and gypsum in the GJAST-20-10 location.

4.1 Selective Extractions

4.1.1 Data

Data from the selective extractions are provided in Appendix C, and solid-phase concentrations are reported in micrograms per gram (µg/g), which is equivalent to mg/kg, or ppm. These include uranium concentrations from carbonate leaching (Table C-1), 5% nitric acid leach (Table C-2), microwave digestion (Table C-3), and total digestion (Table C-4) on all sediment samples. Note that some original sediment samples had to be combined (especially samples below the water table) into one sediment sample due to low sample recovery. In Appendix C, any combined samples are indicated with more than one sample depth in the ID number (i.e., 7-22,23 is a combined sample from a depth of 22 and 23 feet below ground surface). The 5% nitric acid leaching also included analyses for molybdenum and manganese. Iron concentrations were measured on samples that were used for column testing using an ammonium oxalate extraction (Table C-5). Iron concentrations were also measured using carbonate leaching (Table C-1), 5% nitric acid leach (Table C-2), microwave digestion (Table C-3), and total digestion (Table C-4) on just the samples that were used for column testing. A summary of the solid-phase iron concentrations for the column test samples compared to those for uranium, manganese, and molybdenum is provided in Table C-6. As discussed in the digestion methods (Section 3.2), the ammonium oxalate extraction is designed to measure noncrystalline iron, whereas the total digestion measures all the iron in the sample, which is a much higher value (Table C-6). Likewise, the 5% nitric extraction likely extracts noncrystalline iron, molybdenum,

and manganese. The microwave extraction appears to dissolve a majority of the iron present in the tested samples, but the concentration is not as high as that of the total digestion (Table C-6).

Appendix C provides a series of graphs for locations GJAST-01 through GJAST-22 with uranium in the solid phase from extraction by carbonate leach, 5% nitric acid leach, microwave digestion, and total digestion. All these graphs plot the solid-phase uranium concentrations with depth based on sample elevation. For comparison, all of these graphs use the same scale for uranium concentration and sample elevations. A second series of graphs for locations GJAST-01 through GJAST-22 provides the available data for molybdenum, manganese, and iron by 5% nitric acid leach and iron by ammonium oxalate leach compared to uranium by 5% nitric acid leaching. These graphs also plot the solid-phase concentrations with depth based on sample elevation and use the same scale for sample elevations. Given the large range in concentrations, the scales for solid-phase concentrations are not always the same.

4.1.2 Method Comparisons

From the Appendix C graphs on uranium concentrations in the solid phase, it is easy to visually see the order of increasing aggressiveness of the leaching procedures reflected in the uranium concentrations going from carbonate leach to 5% nitric acid leach, to microwave digestion, to total digestion (also see Figure 5). While it is not possible to evaluate the exact mineral association for each leach/extraction procedure without pre- and post-sampling, the following is a general guide with median uranium values from the full data set:

- Carbonate leach: removes loosely sorbed (labile) uranium (median U concentration = 0.62 mg/kg)
- 5% nitric acid leach: removes all sorbed uranium and possibly some precipitated uranium (median U concentration = 1.16 mg/kg)
- Microwave extraction: More aggressive than the 5% nitric acid leach such that any uranium not associated with mineral grains is dissolved (median U concentration = 1.79 mg/kg)
- Total digestion: dissolves all mineral grains and, thus, measures total uranium content (median U concentration = 3.37 mg/kg)

Overall, it appears that the uranium content from the microwave digestion is between the 5% nitric acid leach and the total digestion values (Appendix C). Some of the microwave digestion results are similar to the total digestion results, and a few actually exceed the total digestion results (Figure 5). Microwave digestion results that are similar to the total digestion results may indicate that the microwave digestion actually melted some mineral grains. The microwave digestion results that exceeded the total digestion results indicate grain melting along with higher uranium concentrations due to slight measurement error and/or likely sample variability between split samples.

Previous background data at three locations along the Gunnison River included sediment data collected just south of the Grand Junction site (DOE 2002). These samples were analyzed after the use of microwave digestion, and the uranium concentrations were 1.0, 0.83, and 1.2 mg/kg. For comparison, in location GJAST-03 the microwave digestion median uranium value was 1.28 mg/kg, and it appears that the uranium values in GJAST-03 are fairly representative of background values (Figure 5).

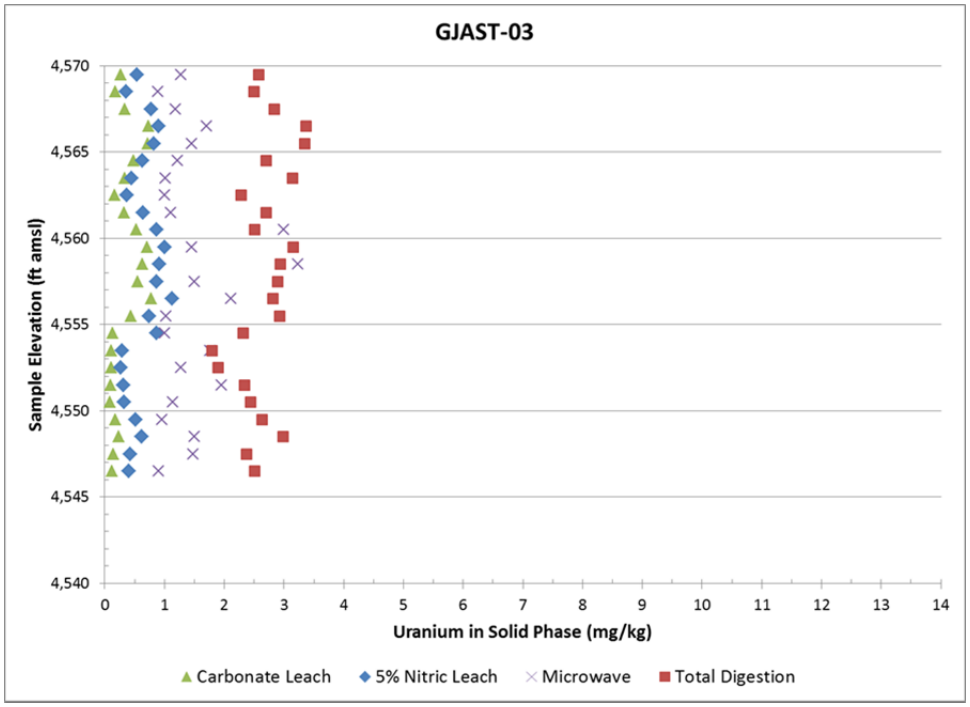

Figure 5. Results of Selective Extractions and Total Digestion for Location GJAST-03

Before evaluating any plume persistence issues in groundwater, the amount of mill-related uranium in the solid phase that can be readily released should be evaluated from an available mass standpoint. In general, the 5% nitric acid leach should dissolve any secondary uranium compared to a total digestion of all uranium present. Secondary uranium is defined as any sorbed or precipitated uranium that is not associated with an original rock or mineral grain. The subtraction of these two should give the amount of primary uranium that is likely present in the original mineral grains. For the entire data set where total digestion data are available, the difference between the total digestion and the 5% nitric acid leach averages 2.21 mg/kg for uranium, which can be considered the average amount of primary uranium present in the original mineral grains. For comparison, this value is quite similar to the average worldwide crustal abundance of uranium near 2.7 mg/kg (Taylor 1964).

The GJAST-03 location appears to be relatively uncontaminated compared to other samples in the data set and the background samples from DOE (2002). GJAST-03 has a median total digestion value of 2.67 mg/kg uranium compared to the 5% nitric acid leach with a median value of 0.62 mg/kg uranium, for a difference of 2.05 mg/kg uranium (also see Figure 5). The value of 0.62 mg/kg uranium from the 5% nitric acid leach in location GJAST-03 may be considered that of naturally occurring secondary uranium, and values above this concentration are likely due to a mill-related uranium source. From a graphical perspective, it is relatively quick and easy to scan the graphs in Appendix C for 5% nitric acid leach results and identify samples that appear to have mill-related secondary uranium by comparing them to a background value of <1 mg/kg uranium. The same could be done for the carbonate leach at a slightly lower value or the microwave and total extractions at higher values. However, the 5% nitric acid leach values provide a good approach for estimating the total amount of secondary uranium that is likely mill-related and that could be released into the groundwater, thus creating plume persistence issues if released.

4.1.3 Significance of the Water-Table Elevation

At nearby well 8-4S (Figure 3 and Figure 4), the median groundwater elevation between 2013 and 2016 was 4557 ft above mean sea level (amsl). Past water-table elevations in well 8-4S are shown in Figure 6 and Figure 7. Mill tailings at the Grand Junction site were removed in the time period of 1989 to 1994 (DOE 2016); thus, the higher groundwater elevations before 1994 may have been associated with the presence of mill tailings in the area that were more permeable to recharge than the surrounding surficial silt layer.

Many of the GJAST borehole samples show distinctly higher uranium concentrations above the median groundwater elevation and uranium concentrations near background below the median groundwater elevation (Appendix C and GJAST-14 as an example, Figure 8). Exceptions to this are at locations GJAST-15 (Figure 9), where an organic carbon-rich zone was identified at 4554–4556 ft amsl and GJAST-20 (Figure 10) where gypsum was detected in sample GJAST-20-10 (elevation of 4558.2 ft amsl). Gypsum may also occur in samples above and below GJAST-20-10, but XRD analyses were not completed on those samples. Gypsum is a likely indicator of water inflow from the mill tailings where calcite dissolves and buffers the incoming low-pH water. This reaction, along with high sulfate content dissolved from the tailings, produces gypsum precipitation. Whether or not the gypsum precipitation provides a mechanism for longer retention of uranium below the water table is unknown. However, the active precipitation of gypsum during contaminated water inflow, along with any ongoing iron hydroxide precipitation that can provide uranium sorption surfaces, may provide a coating mechanism that would protect uranium for subsequent release.

An increased uranium content above or below the water table is not seen in locations GJAST-02, GJAST-03 (Figure 5), GJAST-05, and GJAST-12 (Appendix C). GJAST-22 only shows a slight uranium increase near the ground surface (Appendix C). In these samples, the uranium content is generally near 1 mg/kg or less for the carbonate leach and the 5% nitric acid leach. The microwave digestion uranium values are more variable but are generally less than 2 mg/kg. For total digestion, the uranium values are near 3 mg/kg. In general, these five boreholes appear to be relatively uncontaminated.

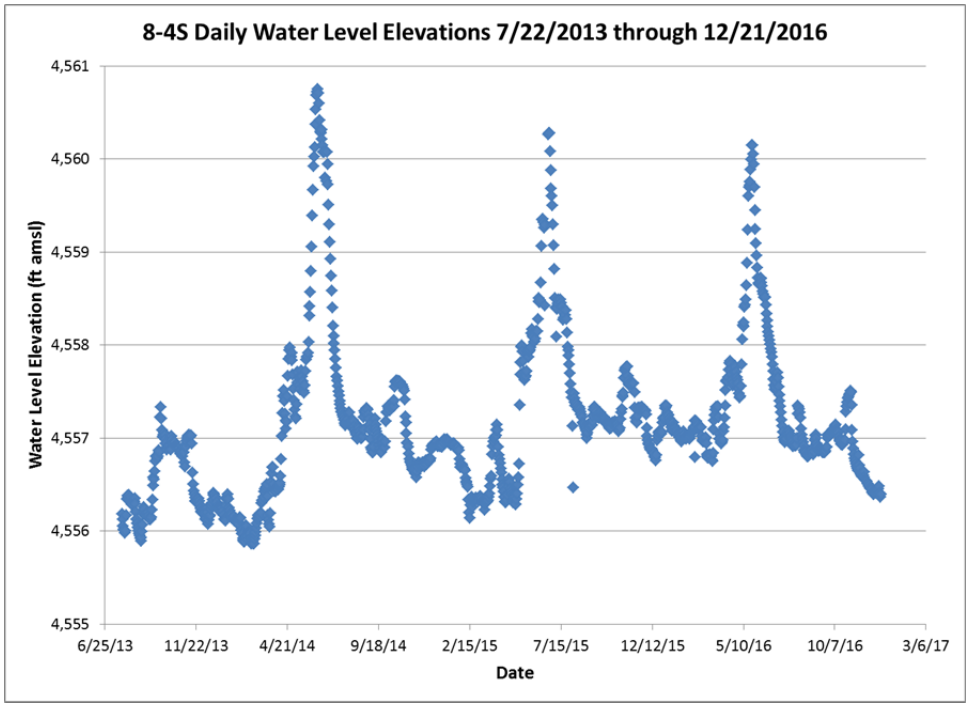

Figure 6. Graph of Daily Water-Level Elevations for Well 8-4S

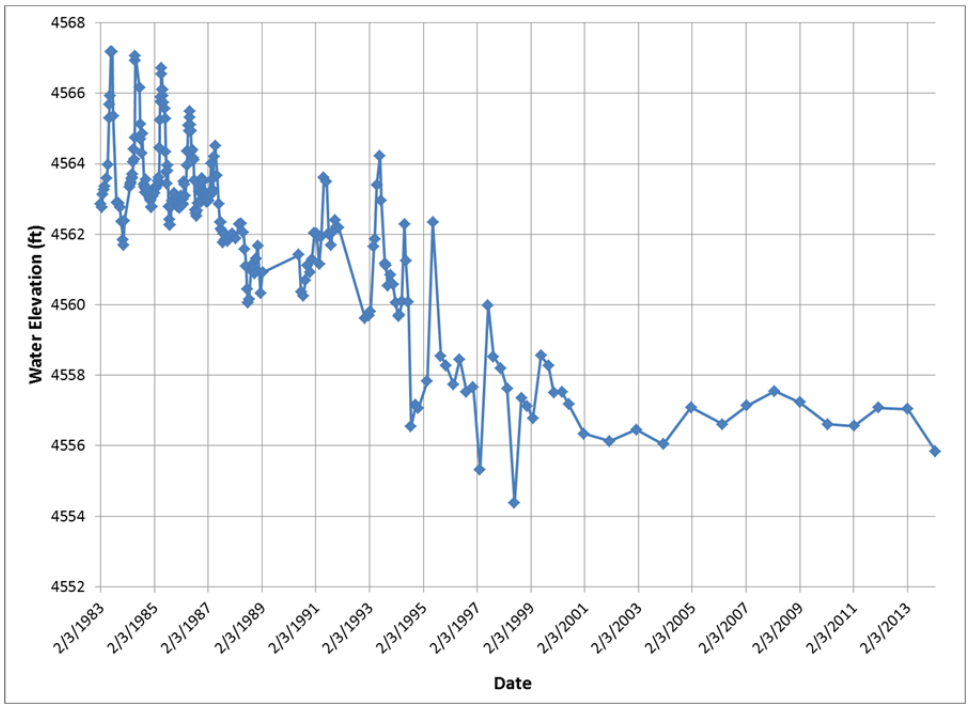

Figure 7. Historical Graph of Water-Level Elevations for Well 8-4S

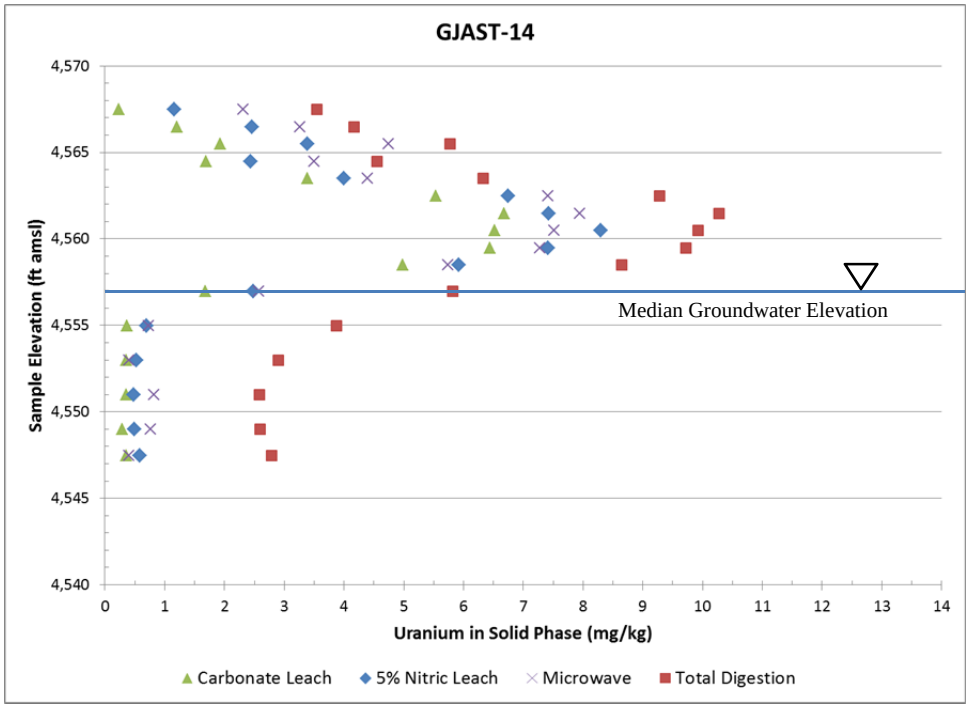

Figure 8. Results of Selective Extractions and Total Digestion for Location GJAST-14

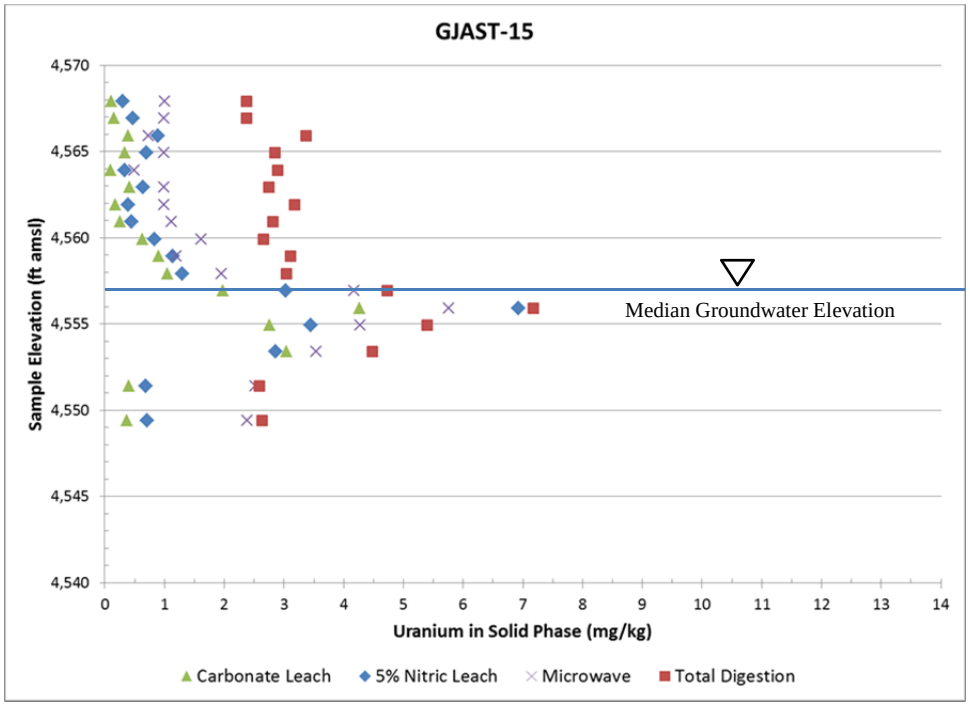

Figure 9. Results of Selective Extractions and Total Digestion for Location GJAST-15

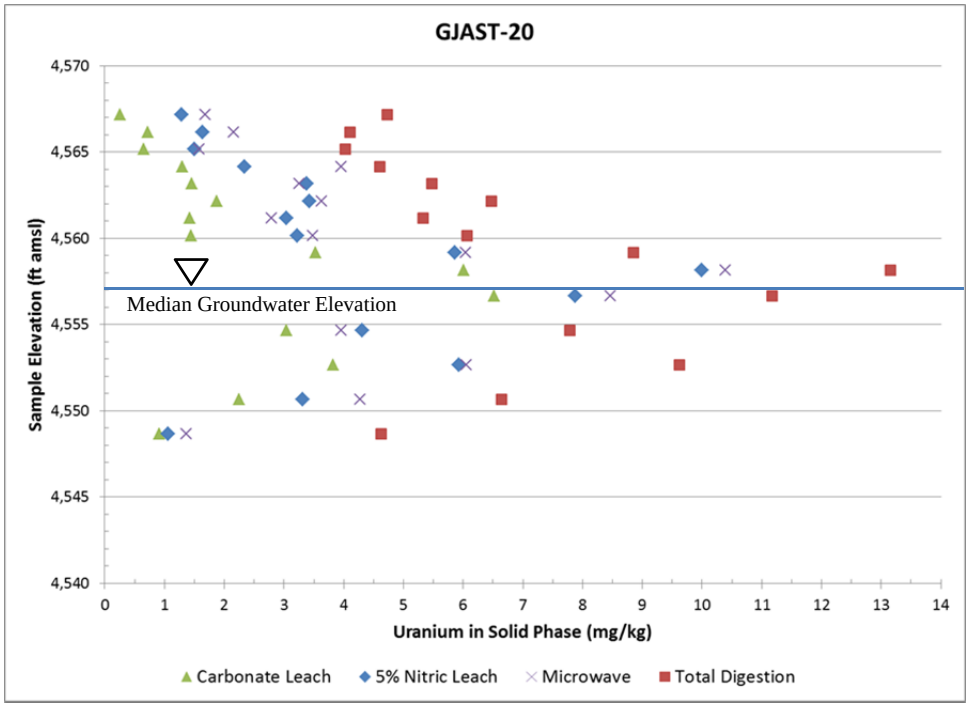

Figure 10. Results of Selective Extractions and Total Digestion for Location GJAST-20

4.1.4 Molybdenum, Manganese, and Iron

In addition to uranium, all of the samples for 5% nitric leach also had analyses for molybdenum and manganese (Appendix C). Distinct trends in molybdenum and manganese with depth are not very apparent, but manganese concentrations do seem to decrease with depth. When compared to uranium concentrations from the 5% nitric acid leach, uranium concentration is usually greater than that of molybdenum above the water table and similar in concentration below the seasonal water-table median (Appendix C and Figure 11 as an example). The concentration correlations of uranium with manganese and molybdenum with manganese are relatively low and produce *R* squared values of 0.0169 and 0.0116, respectively.

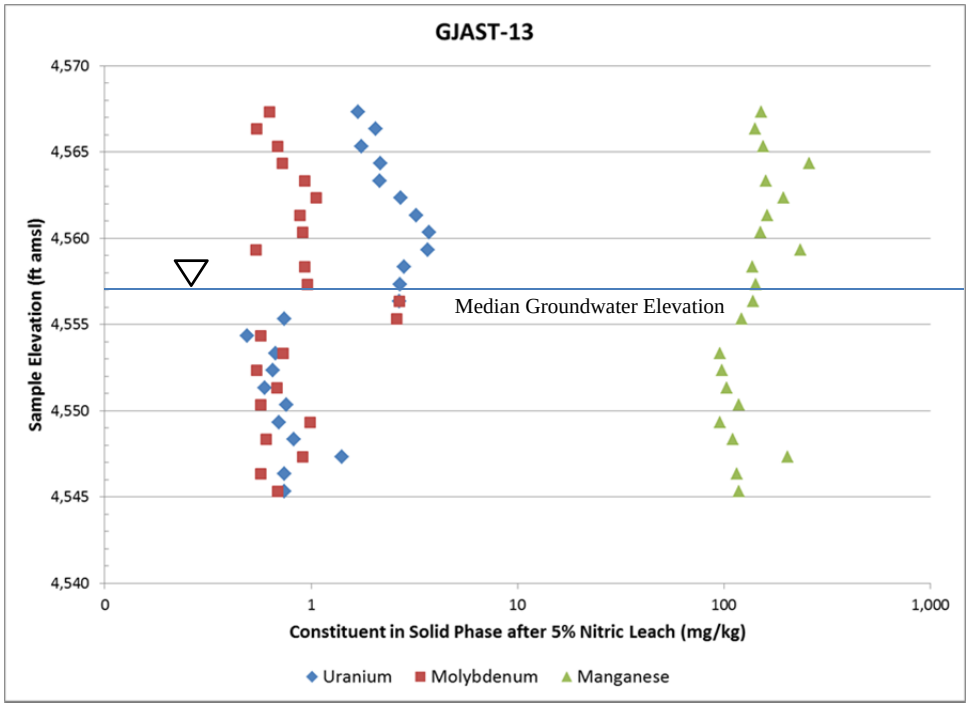

Figure 11. Results of Selective Extractions and Total Digestion for Location GJAST-13

Iron concentrations were measured on all the samples used for the column tests and included iron data from all the extraction techniques (total digestion, carbonate leach, ammonium oxalate leach, 5% nitric acid leach, and microwave digestion). These data are summarized in Appendix C, Table C-6, along with the uranium, molybdenum, and manganese extraction data. For the iron extractions, the increased leaching aggressiveness is in order of ammonium oxalate to 5% nitric acid leach then microwave digestion. All three of these techniques can provide iron concentrations related to fresh or aged precipitates of iron oxyhydroxides that could sorb uranium and molybdenum. Thus, iron was measured on the column test samples as a possible indicator of the potential for uranium and molybdenum sorption and a subsequent control on mobility during the column tests. Unfortunately, the iron extraction data is too limited to determine any significant trends or correlations with other elements. However, the iron concentrations from the ammonium oxalate extraction do appear to increase with depth (Appendix C).

4.1.5 Three-Dimensional Stickball Images

Three-dimensional "stickball" images were created for the uranium concentrations from the 5% nitric acid leach data (Figure 12). This image uses the data from Appendix C and plots all the uranium concentrations with depth with a concentration-based color coding. Figure 12 highlights the higher uranium concentrations seen in locations GJAST-14, GJAST-19, and GJAST-20.

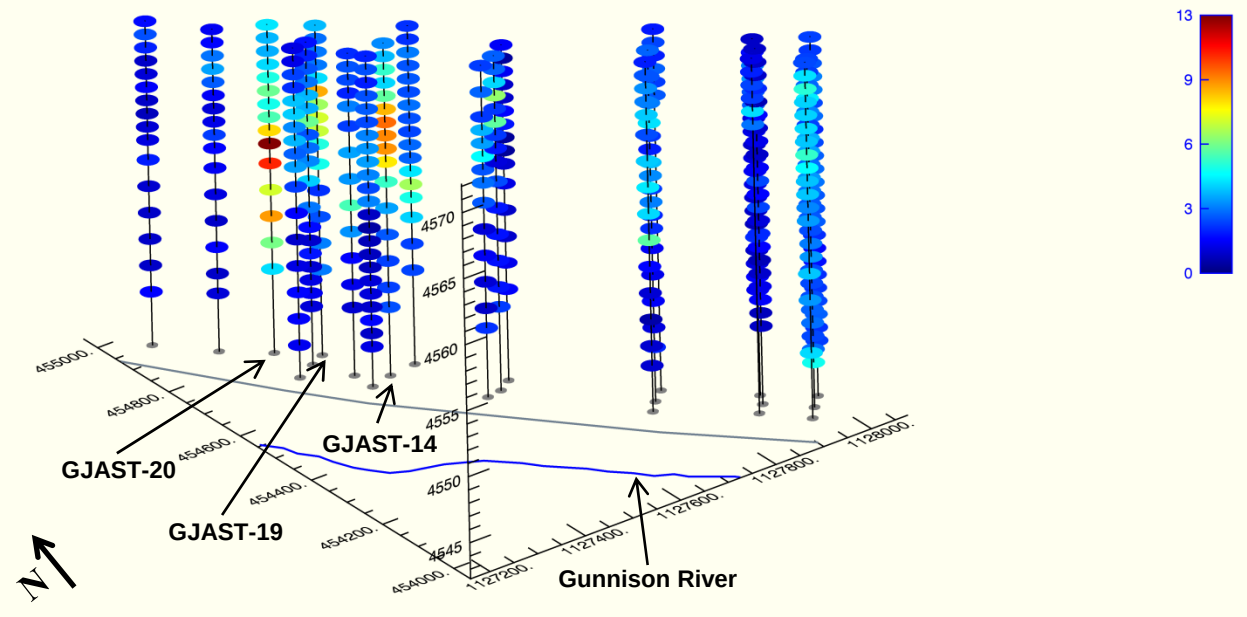

Figure 12. Three-Dimensional Stickball Views of Uranium Concentrations from the 5% Nitric Acid Leach in mg/kg

4.2 Column Testing

4.2.1 Small Columns Without Full Geochemistry

All column test data can be found in Appendix D, which includes a table for each column and graphs with the resulting uranium concentrations compared to pore volumes. The black square points in the graphs in Appendix D indicate the pore volume just before a stop-flow test was completed. A list of the tested columns (Table 7) provides a summary of the small column data with the peak uranium concentrations in the column effluent compared to the solid-phase uranium concentrations for the various leaching and digestion tests. To compare uranium flushing rates, Table 7 also includes the number of pore volumes necessary for the uranium concentration to reach 400 µg/L. This value was selected to get a quantitative comparison of flushing rates between the columns based on pore volumes, and 400 µg/L was selected as a value that was reached in the majority of the columns in the 7–10 pore volume range. For reference, the maximum contaminant level (MCL) standard for uranium at LM sites is 44 µg/L. The measured analyte concentrations for the lab-prepared influent water are listed in Table 8. The measured range of values is due to the multiple batches that were created throughout the column testing and is compared in Table 8 to the target concentrations from the added solid phases that are listed in Table 4.

Table 7. Summary of Small Column Data

Core Sample Number	Carbonate Leach Uranium (mg/kg)	5% Nitric Acid Leach Uranium (mg/kg)	Total Digestion Uranium (mg/kg)	AmmOx Iron (mg/kg)	Peak Column Effluent Concentration Uranium (µg/L)	Approximate Pore Volumes for Flushing to 400 µg/L Uranium	Initial Flow Rate (mL/min)
14-7	6.68	7.43	10.28	870	6269	9.1	0.09
14-8	6.53	8.30	9.92	792	6994	9.5	0.09
14-9	6.44	7.41	9.73	809	6299	9.4	0.09
14-19	0.29	0.49	2.60	3030	336	0.0	0.10
15-13	4.27	6.93	7.18	3175	1594	23.0	0.04
19-6	5.08	6.24	9.45	770	1985	30.0	0.03
19-8	4.44	5.69	7.80	1398	2395	8.3	0.09
19-9	4.14	4.94	7.63	1551	2682	7.5	0.10
19-15	0.37	0.63	2.79	2794	345	0.0	0.10
20-9	3.53	5.86	8.85	660	2,76	7.2	0.09
20-10	6.01	9.99	13.16	948	6113	15.0	0.08
20-11	6.52	7.88	11.17	1676	2494	31.0	0.08
20-15	3.82	5.93	9.63	3690	1277	13.5	0.10

Abbreviations:
AmmOx = ammonium oxalate leach
µg/L = micrograms per liter
mg/kg = milligrams per kilogram
mL/min = milliliters per minute

Table 8. Column Test Influent Water

Analyte	Target	Measured Range for Small Columns	Measured Range for Large Column	Values for Large Column Used in Modeling
pH	7.0	7.0	7.0	7.0
Alkalinity (mg/L as $CaCO_3$)	300	309 to 314	313	313
Total organic carbon (mg/L)			9.1	
Cl (mg/L)	87.31	79.9 to 86.0	79.6 to 89.0	86.7
Sulfate (mg/L)	905.5	929 to 966	904 to 934	918
Mg (mg/L)	61.45	62.2 to 68.5	61.0 to 61.1	62.8
Ca (mg/L)	197.4	197 to 208	185 to 193	192
Na (mg/L)	300.0	306 to 334	291 to 306	298
K (mg/L)	8.53	8.9 to 9.8	8.7 to 9.3	8.82

All of the columns show an initial peak in uranium release, with a single initial peak for columns 19-8, 19-9, 19-15, and 20-11 (19-8 is duplicated here in Figure 13 as an example); a delayed uranium peak for 14-7, 14-8, 14-9, 15-13, 20-9, 20-10, and 20-15 (14-9 is duplicated

here in Figure 14 as an example); and a unique trend for column 19-6 with a peak uranium concentration followed by lower uranium concentrations, another peak, and then a slow decline (Figure 15).

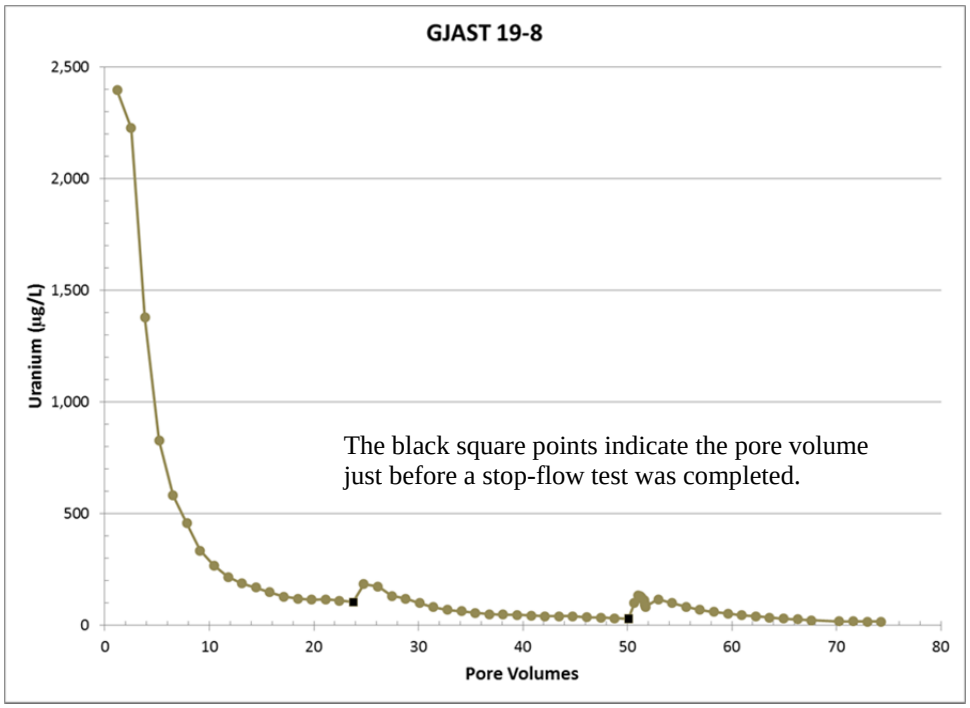

Figure 13. Column Data for Location GJAST-19-8

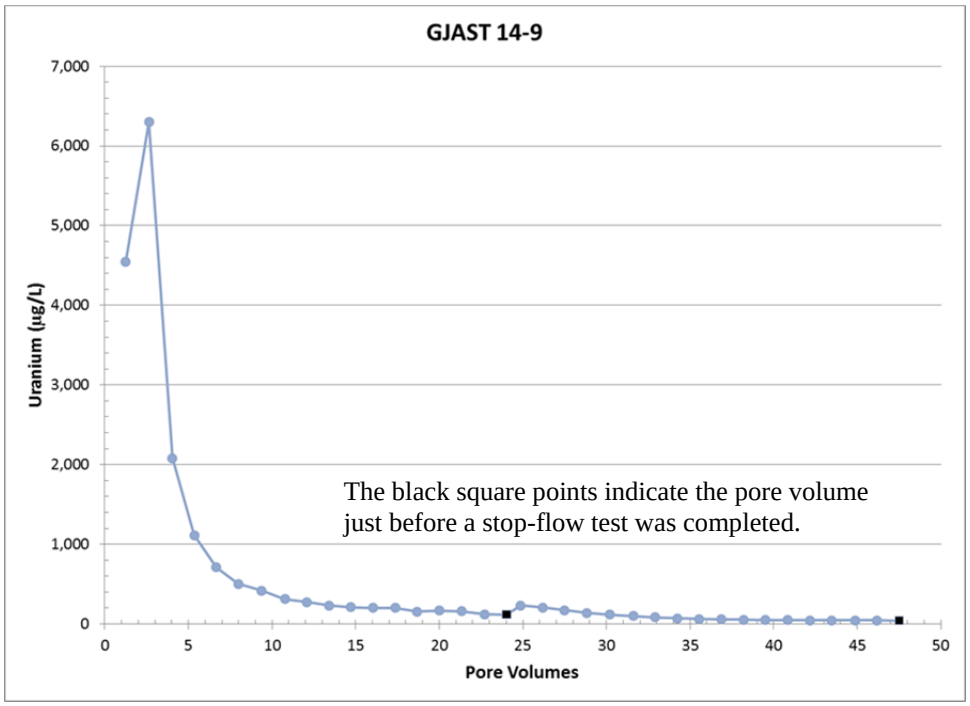

Figure 14. Column Data for Location GJAST-14-9

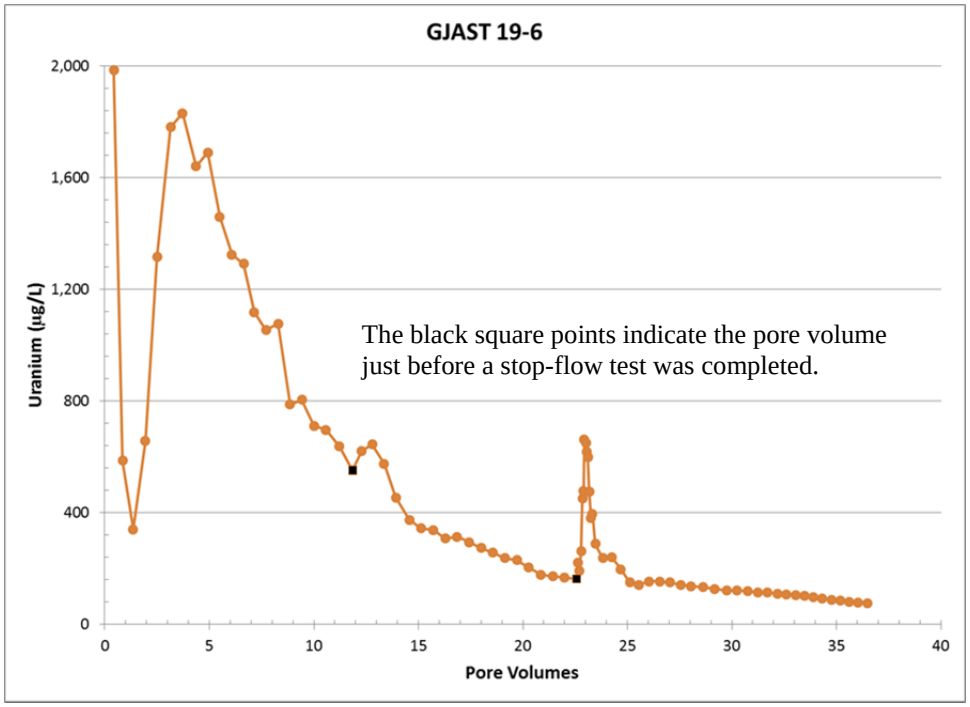

Figure 15. Column Data for Location GJAST-19-6

All the columns showed nonequilibrium conditions during stop-flow events where uranium rebounded during the stop-flow event and then resumed flushing when flow was restarted. For column 19-6 (Figure 15), the large uranium rebound was due to an extended column flow disruption while a plugging issue was resolved.

Data indicate that the overall uranium concentration strongly controls the amount of peak uranium released during the column test (Table 7). Columns 14-19 and 19-15 had much lower peak uranium concentrations that were consistent with much lower uranium derived from the carbonate leach, 5% nitric acid leach, and total digestions. The number of pore volumes required to reach 400 µg/L for uranium concentrations in column effluent water provides information on the uranium flushing rate. The greater number of pore volumes to reach 400 µg/L uranium in the outflow water for columns 15-13 and 19-6 appears to be due to slower flow rates (Table 7). The reasons for the slightly slower uranium flushing rates for columns 20-10, 20-11, and 20-15 are unclear. However, the previously mentioned detection of gypsum in sample 20-10 could have created a gypsum mineral coating that influenced the release of uranium. XRD data is only available for sample 20-10, but the presence of gypsum in samples 20-11 and 20-15 is possible. When the tailings were weathering, this uranium may have been incorporated into the gypsum or sorbed to iron oxyhydroxides that were then coated by gypsum. Thus, the release of uranium may be controlled by the dissolution of gypsum. Overall, the release of uranium from the smaller cores without complete geochemical analyses is difficult to explain with just uranium concentrations. However, all of these columns do show slow release of uranium that can lead to plume persistence issues that can maintain uranium in the groundwater above MCLs. Section 4.4 on reactive transport modeling uses data from a larger column to interpret the potential controls on uranium release.

4.2.2 Larger Column for Sample GJAST 20-10 with Full Geochemistry

Split samples of location GJAST 20-10 were tested in small and large columns to compare results with different column sizes. The flow rate in the small column was approximately 0.075 to 0.080 mL/min compared with 0.10 to 0.15 mL/min for the large column (target flow rate was 0.15 mL/min). Even with these flow rate differences, the uranium concentrations in the column effluent per pore volume were quite similar (Figure 16). Both tests included stop-flow tests at 25 and 50 pore volumes, with similar results in rebounding uranium concentrations, even though the stop-flow times in the larger column were about 2.5 times longer in duration. These results indicate nonequilibrium conditions between the mobile water phase and the solids at both flow rates. As a result, when flow is discontinued, uranium continues to be transferred from the solid phase to the water phase until the flow is restarted.

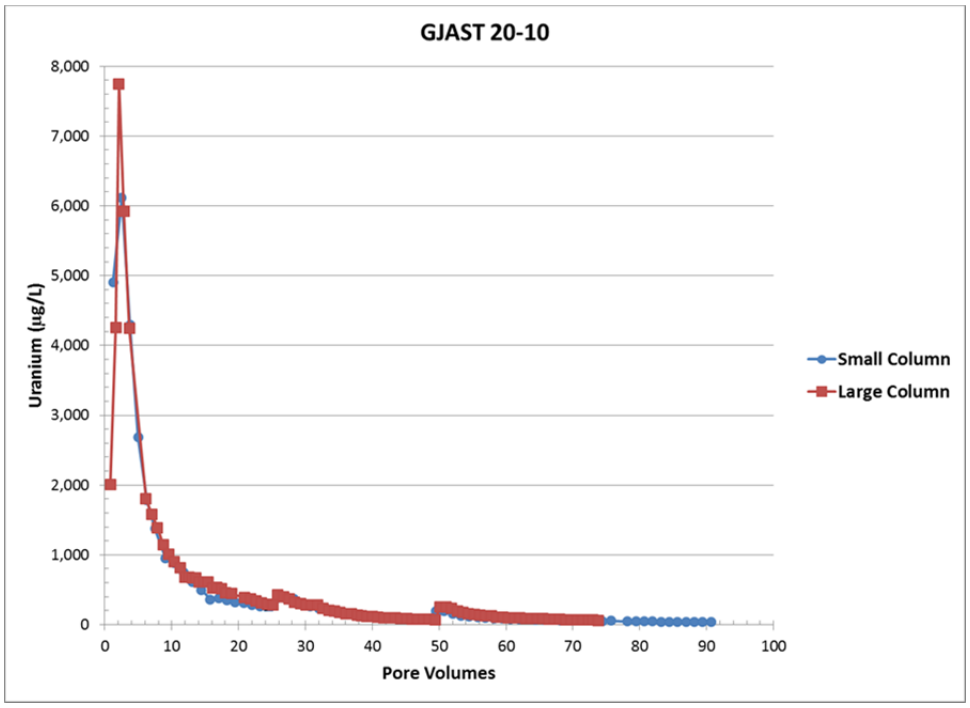

Figure 16. Uranium Concentrations with Pore Volumes for Small and Large Columns Using Sample GJAST 20-10

The main advantage of the larger column was the larger water volume allowed for analyses of additional constituents. These included pH and sulfate (Figure 17); total organic carbon (TOC), chloride, and potassium (Figure 18); alkalinity (alk), magnesium, calcium, and sodium (Figure 19); and iron and manganese (Figure 20). The pH was slightly variable within a range of 7.55–8.15 throughout the test. TOC and Na flushed out of the column within 5 pore volumes. Potassium shows a slow decline in concentrations for 30 pore volumes before it reaches influent concentrations. Chloride concentrations remained similar to those of the influent water through the test, and therefore, chloride was likely not present in the solid phase. Iron and manganese were not added to the influent water, and the column test showed some iron and manganese in the effluent water, but not in significant amounts. Alkalinity increases from the first sample at 101 mg/L as $CaCO_3$ to near the influent concentration of 300 mg/L as $CaCO_3$ at 7 pore volumes. Calcium remained at around 600 mg/L until 60 pore volumes, and then it decreased to near the

influent concentration of 300 mg/L. Sulfate concentrations declined initially, leveled off at around 2000 mg/L, and then decreased again after 60 pores volumes. The decrease in calcium and sulfate at 60 pore volumes is likely related to the dissolution of gypsum. XRD data confirmed the presence of gypsum in the GJAST 20-10 sample.

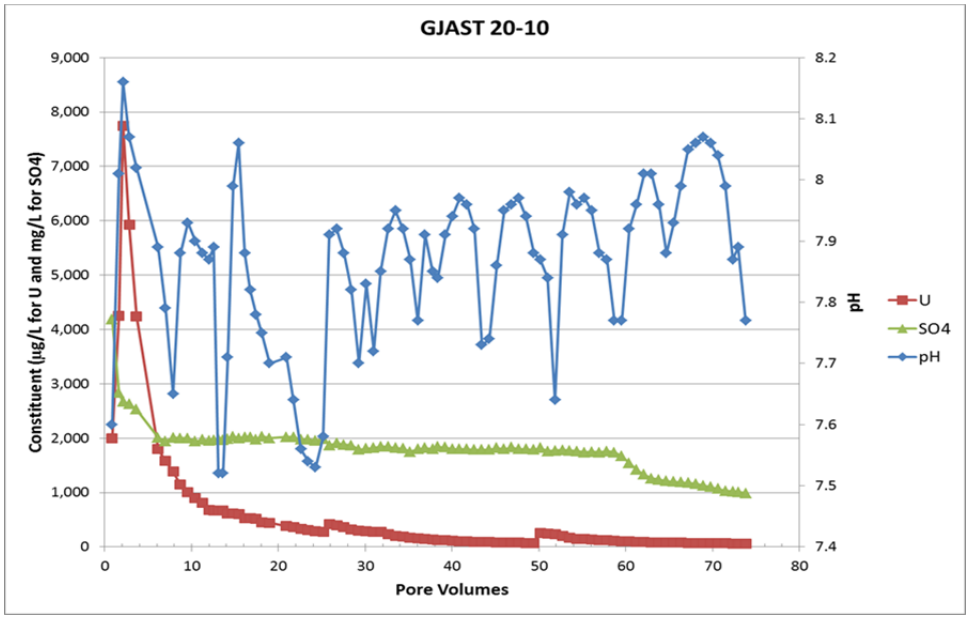

Figure 17. Large Column Data for Location GJAST 20-10: pH, Sulfate, and Uranium

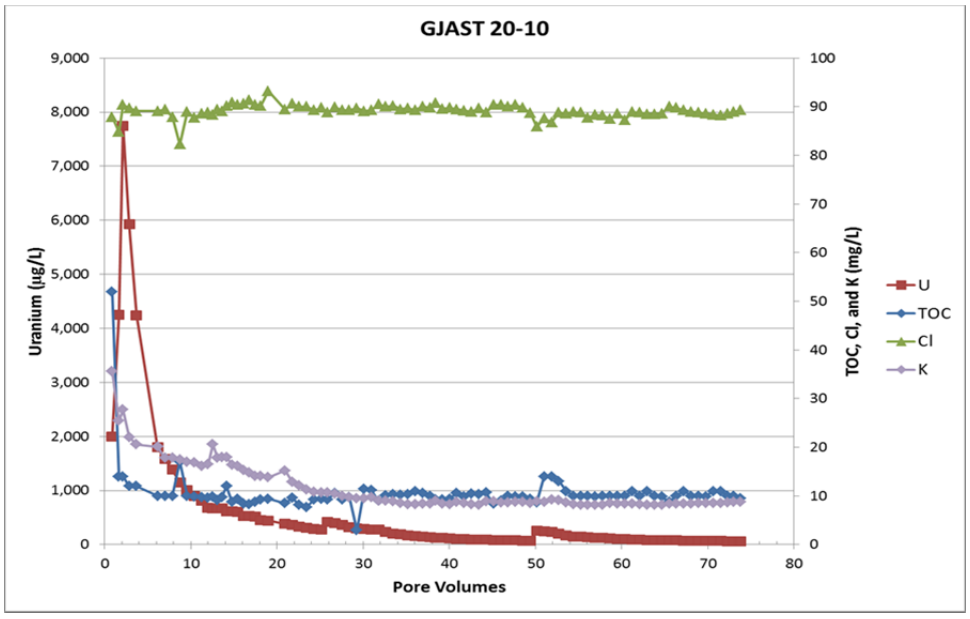

Figure 18. Large Column Data for Location GJAST 20-10: Uranium, Total Organic Carbon, Chloride, and Potassium

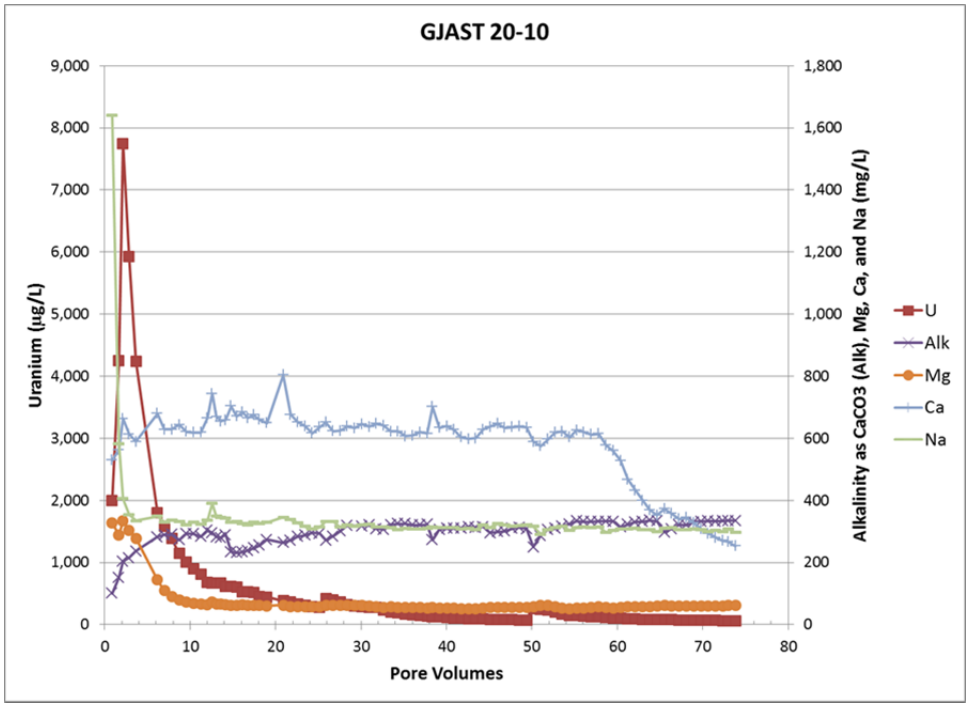

Figure 19. Large Column Data for Location GJAST 20-10: Uranium, Alkalinity, Magnesium, Calcium, and Sodium

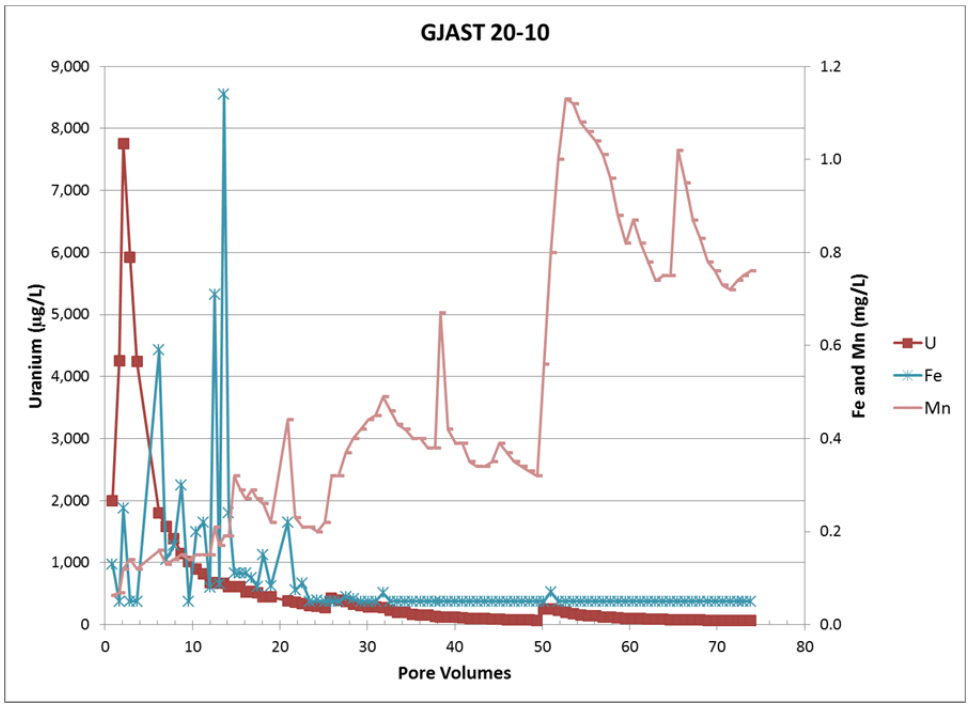

Figure 20. Large Column Data for Location GJAST 20-10: Uranium, Iron, and Manganese

4.3 Petrography and Fission-Track Radiography

Images from the thin sections and fission-track radiography are provided in Appendix E. These images compare the fission-track radiography results with plain light, oblique light, reflected light, or imagery through crossed Nicol prisms. Each type of light can assist in the identification of different minerals. However, for this report, the focus is more on grain coatings and cements than on the identification of individual minerals. Thus, the different lighting was mainly used to enhance the imagery of grains versus coatings and cements. Imagery is provided for samples GJAST 14-8, 15-13, GJAST 20-10, and GJAST 20-11, with the majority of images from GJAST 20-10 (sample with the highest uranium content). The fission-track radiography shows the locations where uranium occurs in comparison to the mineral grains. More fission tracks indicate more uranium in an individual sample, but fission track amounts cannot be compared between samples due to possible variations in irradiation strength, mica thickness, and development time.

The results can be simplified into four categories where more fissions tracks indicate relatively more uranium: (1) more fissions tracks seen consistently throughout a mineral grain (Figure 21), (2) more fission tracks seen consistently throughout an organic particle (Figure 22), (3) more fission tracks seen around the outer edge of a grain associated with grain coatings (Figure 23), and (4) more fission tracks seen in intragranular material (Figure 24).

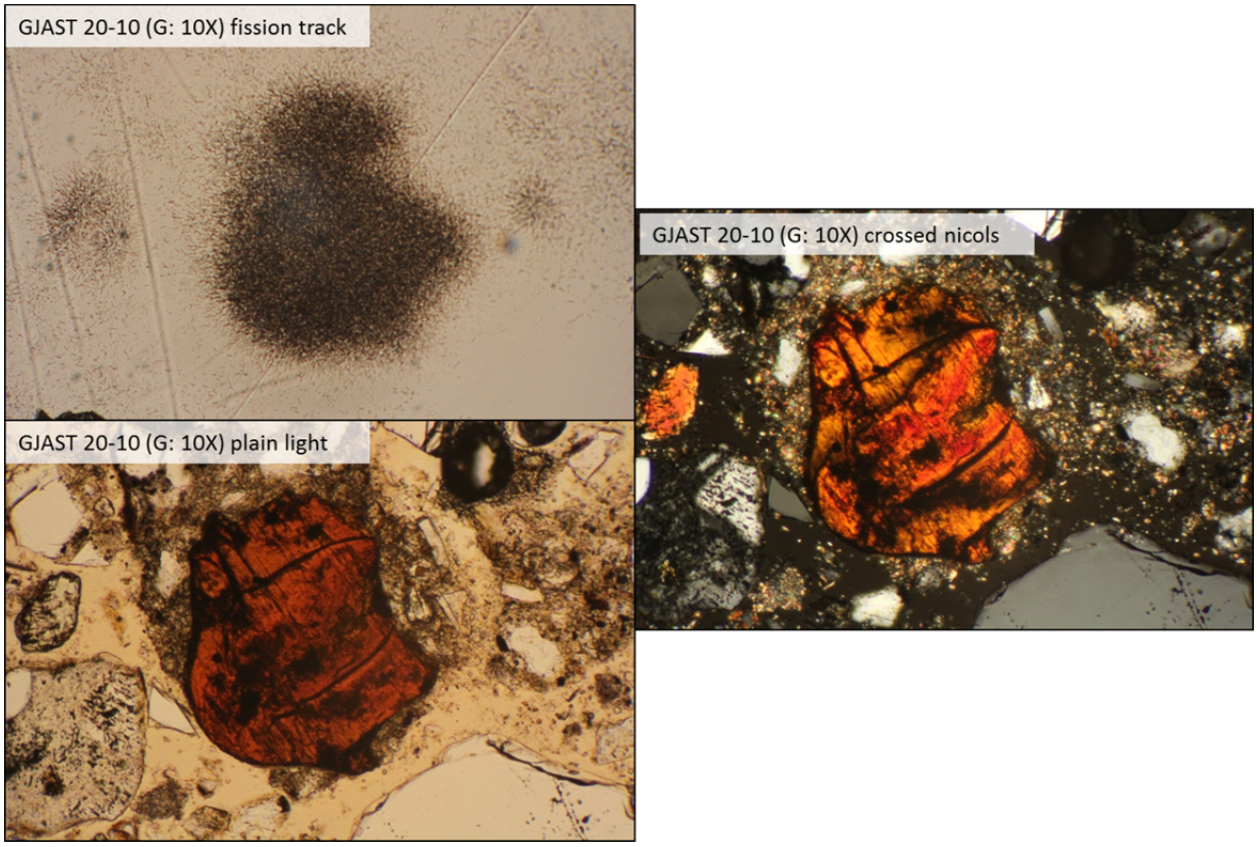

Figure 21. Image of Heavy Mineral Grain (likely monazite) with Fission Tracks Associated with the Whole Grain

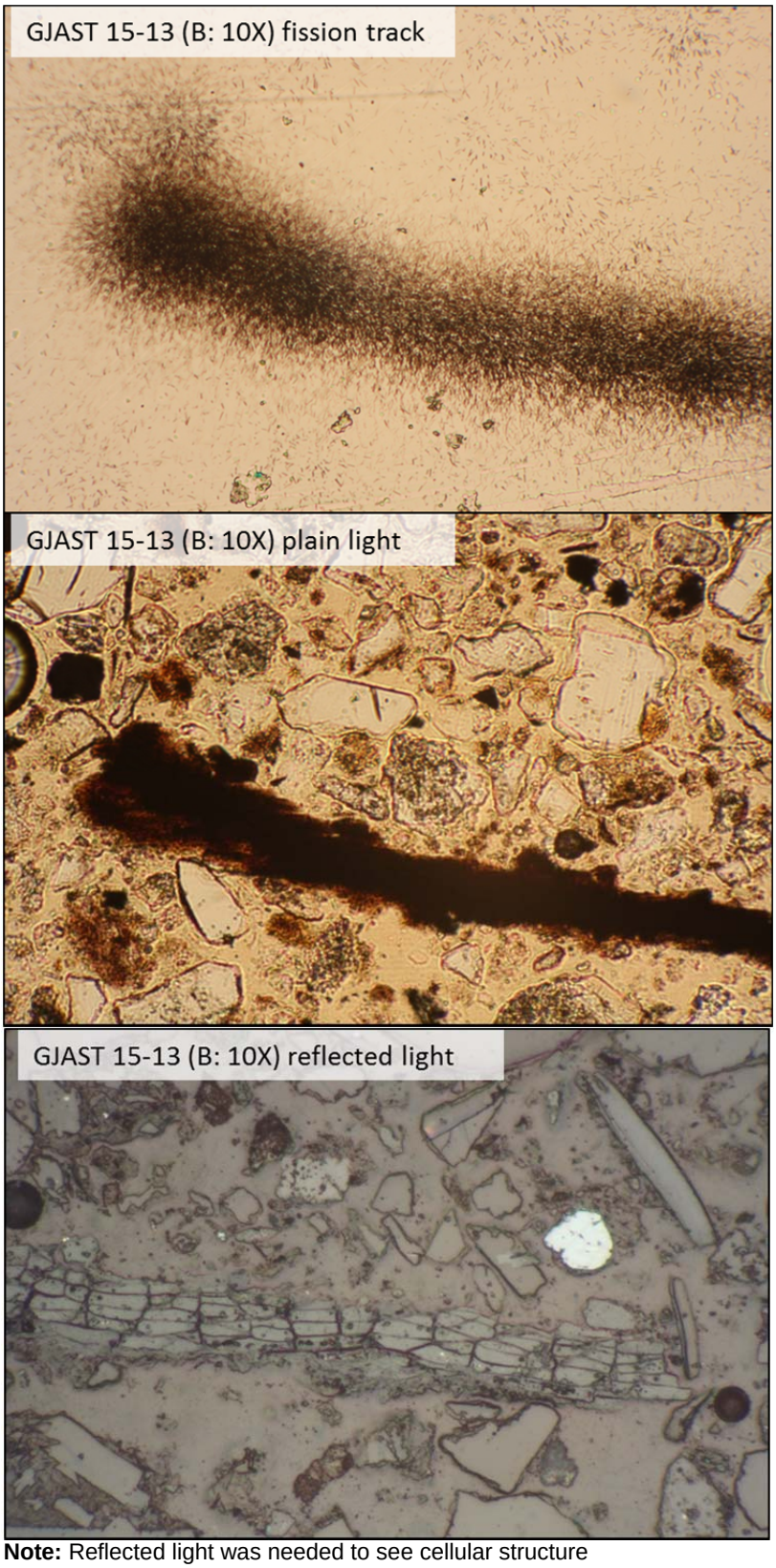

Note: Reflected light was needed to see cellular structure

Figure 22. Images of an Organic Particle with Concentrated Fission Tracks

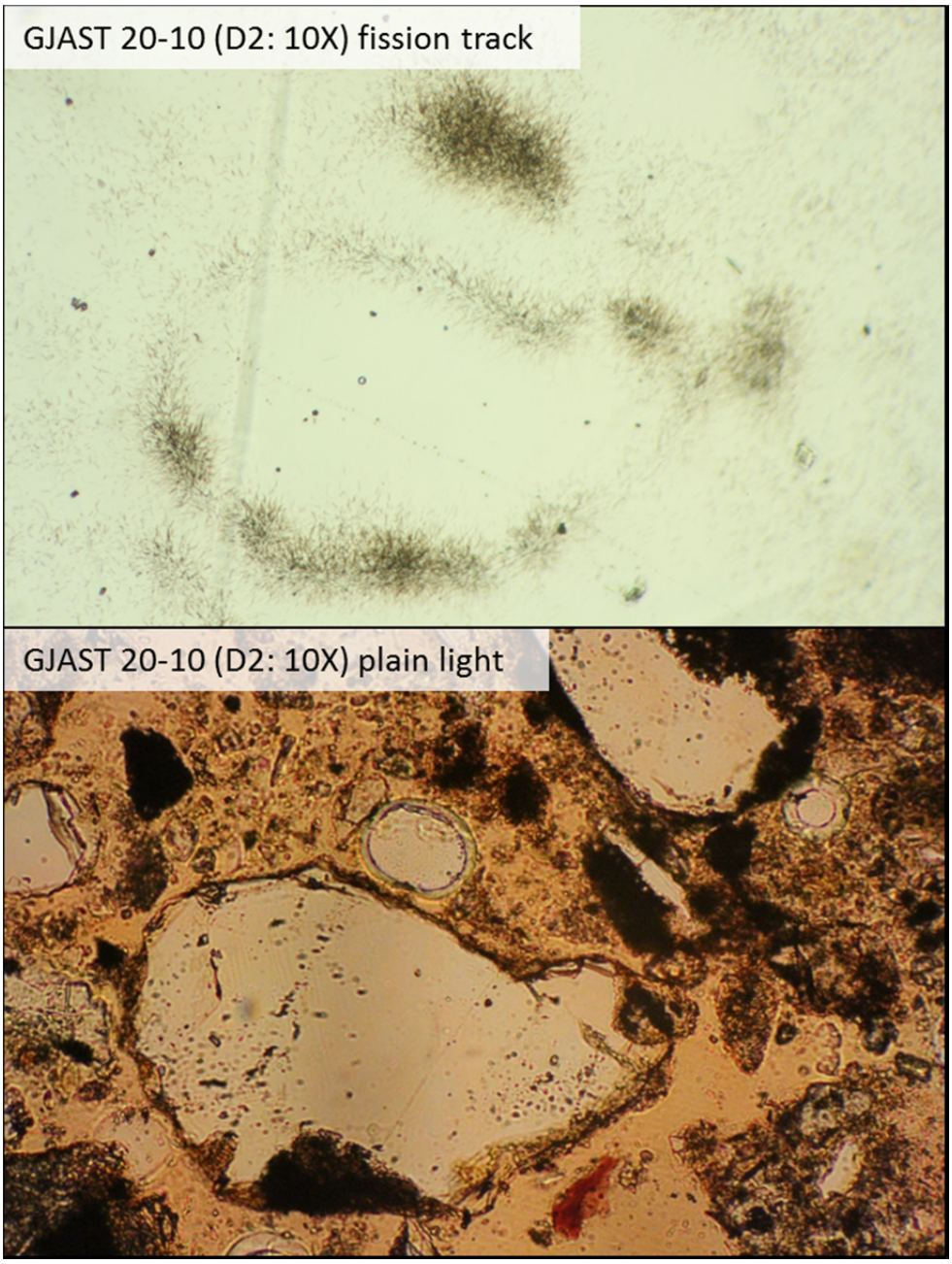

Figure 23. Image of a Quartz Grain with Likely Iron Hydroxide Coatings Where Higher Fission-Track Density is Associated with the Grain Coatings

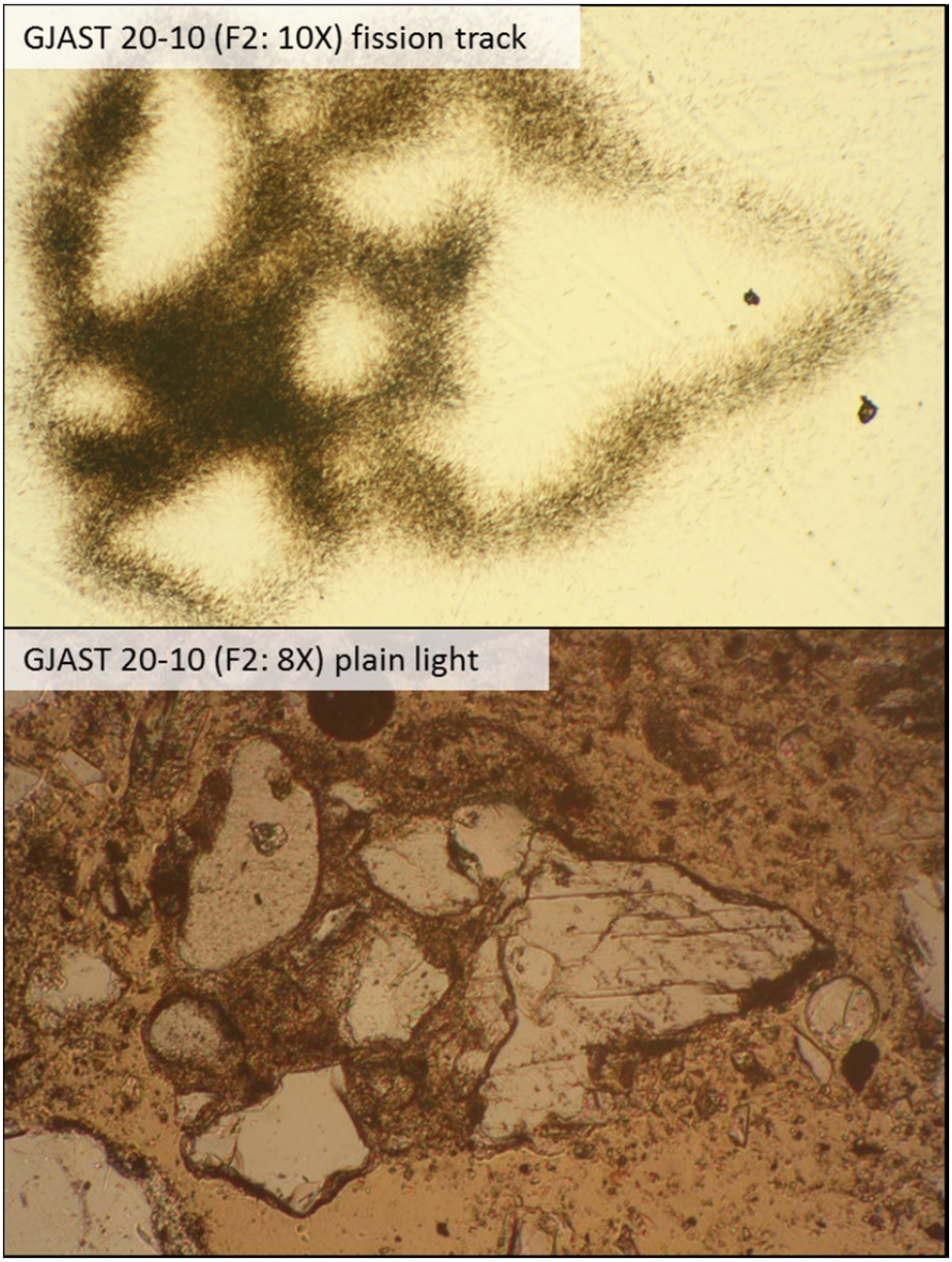

Figure 24. Images of a Larger Grain that is Several Quartz Grains Cemented by Iron Hydroxides and/or Clays with Higher Fission-Track Density Associated with the Cementing Material

The thin sections and fission-track results were not used in a quantitative sense, as that would require a much more detailed analysis. However, the above images do indicate that uranium can be associated with (1) mineral grains, (2) organic particles, (3) mineral coatings, and (4) intragranular cements. Whether or not the uranium with these associations is primary or secondary cannot be determined without additional data, such as uranium-234/uranium-238 isotope activity ratios, where a ratio near 1 is mill-derived uranium and a ratio greater than 1 is naturally occurring uranium. However, mineral coatings and intragranular cements are less likely to be maintained during stream transport in the Gunnison River due to abrasion before deposition on the site floodplain. Thus, it is more likely that the uranium associated with mineral coatings and intragranular cements is related to secondary uranium sorption on precipitated iron oxyhydroxides or preexisting clays, where the uranium and iron are derived from mill-related contamination from water flowing through the tailings.

The fission-track results indicate the possibility of slow release of uranium, especially the intragranular cements, which could contribute to plume persistence. With the selective extraction data, the carbonate leach is likely to remove only the uranium that is loosely bound to mineral coatings, whereas the 5% nitric acid leach does not dissolve individual grains but may dissolve the mineral coatings and intragranular cements. Microwave digestion provides an even stronger digestion that is more likely to dissolve all the intragranular cements and any precipitated uranium. However, the comparison of the selective extraction data with the mineralogy cannot be done quantitatively without addition analyses, such as performing fission-track radiography on samples before and after selective extraction. In any case, the fission-track radiography data provide evidence for the potential of a dual porosity mechanism that can decrease natural flushing rates. In Figure 24, the fission tracks highlight the intragranular cement, which has less porosity than the surrounding sandy aquifer. Outside of the intragranular cement, the groundwater flow velocities are much higher. As a result, natural flushing likely occurs much faster in the main sand and gravel aquifer with areas of greater porosity, with a slower release of uranium in the lower porosity cements. This concept of dual porosity is tested and discussed more in the next section on reactive transport modeling.

4.4 Reactive Transport Modeling

A 1D reactive transport model simulating the GJAST 20-10 larger column with complete geochemistry data was performed using PHREEQC coupled with PEST as discussed in Section 3.6. Since the exact processes that produced the column test results are difficult to determine by just using analytical data trends, the column was modeled using the progressive addition of various geochemical processes, starting simple and getting more complex. These geochemical processes are listed in Table 9, along with abbreviations that are used in presenting these processes. The parameters associated with each process and their initial starting values are listed in Table 10. These starting values were used based on previous modeling work on uranium sorption to oxidized sediments (Johnson et al. 2016a) and initial manual calibration testing without the use of PEST. If the calibration processes produce a unique result, the exact starting values should not be significant. This was tested by using different initial parameter values for the sorp dual gyp model, indicated as sorp dual gyp 2 (Table 11), and is discussed later in this section. The added decimal places in Table 10 and Table 11 are not meaningful but are reported here in order for the modeling results to be accurately reproduced, if ever needed. A PEST input template and control file are provided in Appendix F for the “sorp dual gyp disp CE” model that includes all the geochemical process. This model is provided because all other models can be reproduced from this model by removing the different processes.

Table 9. List of Tested Geochemical Process with Abbreviations and Descriptions

Geochemical Process Abbreviation	Geochemical Process Description
sorp	Generic sorption
dual	Dual porosity
gyp	Add a limited amount of gypsum with saturation index of 0.0 (equilibrium)
Calcite	Add 10 moles of calcite with allowance for dissolution and precipitation with a saturation index of 1.32 (based on column effluent chemistry)
Disp	Dispersion
CE	Cation exchange

Table 10. PHREEQC Modeling Parameters Associated with Each Geochemical Process Along with Initial Starting Values and Units

Geochemical Process	Parameter Abbreviations	Parameter Description	Initial Parameter Value	Parameter Units
Sorption (sorp)	gcsk	Generic complexation, strong sorption sites, log equilibrium constant	5.41601	Unitless
	gcsd	Generic complexation, strong sorption sites, sorption site density	3.192087×10^{-4}	Moles of sorption sites (per 1 kg of water)
	gcssk	Generic complexation, super strong sorption sites, log equilibrium constant	7.33478	Unitless
	gcssd	Generic complexation, super strong sorption sites, sorption site density	6.577990×10^{-5}	Moles of sorption sites (per 1 kg of water)
Dual porosity (dual)	stagdiff	Exchange factor between mobile and immobile cells	4.207449×10^{-6}	1/second
	stagpore	Immobile cells porosity, expressed as a fraction of the total volume (mobile and immobile cells)	0.122385	Unitless
Gypsum (gyp)	gyp	Gypsum amount	0.633573	Moles (per 1 kg of water)
Calcite	none	None	none	None
Dispersion (disp)	disp	Longitudinal dispersivity	8.993204×10^{-3}	Meters
Cation exchange (CE)	exch	Cation exchange capacity	0.174406	Moles of exchange sites (per 1 kg of water)

Table 11. Different Starting Parameter Values for the Second Sorp Dual Gyp Model

Parameter	New Starting Value
gcsk	4.961
gcsd	7.1482×10^{-4} moles
gcssk	8.210
gcssd	9.4511×10^{-5} moles
stagdiff	2.2532×10^{-5} 1/s
stagpore	0.170554
gyp	0.4501 moles

Initial reactive transport modeling with various geochemical processes was completed using a manual calibration where the PHREEQC simulation results were graphically compared to the column test data (Johnson et al. 2016b) before using PEST. This allowed the authors to get a better understanding of how the different geochemical processes influenced the simulation results. This report presents the final simulation results using PEST based on the progressive addition of geochemical processes and provides the final converged PEST parameter estimation values. The tested geochemical processes were completed based on reasonable added complexity, and individual models are listed in Table 12. Table 12 also lists the final sum-of-squared weighted residuals (SOSWR, referred to as phi in the PEST manual) that take the squared difference between each measured and simulated calibration point. PEST allows weighting of calibration points, which is a way to assign relative importance to each point during the calibration process (no weighting was used in these simulations). Thus, the SOSWR values in Table12 provide an overall quantitative value for the goodness of fit between the measured and simulated observation points for each tested geochemical model. These numbers are directly comparable between models because each model uses the same calibration points derived from the column test results.

For a visual reference, in Appendix F the final calibration results are provided for each geochemical process model and each measured constituent. A subset of those graphs is provided in Figure 25 through Figure 38 as part of the following discussion on the modeled combinations of geochemical processes. In addition, Appendix F includes a table of the final converged value for each estimate input parameter and their sensitivities (Table F-1). Table F-2 in Appendix F includes the total phi values (same as the SOSWR) for each geochemical process model along with the phi value related to each geochemical constituent (i.e., uranium, sulfate, calcium, etc.).

Table 12. Summary of Conceptual Models and Goodness of Calibration Fit Based on the Sum-of-Squared Weighted Residuals (SOSWR)

Geochemical Model	SOSWR
sorp	9.82×10^{7}
sorp dual	8.61×10^{7}
sorp gyp	2.43×10^{7}
sorp dual gyp 1	1.01×10^{7}
sorp dual gyp 2	3.61×10^{6}
sorp dual gyp calcite	1.84×10^{7}
sorp dual gyp CE	3.10×10^{6}
sorp dual gyp disp	3.92×10^{6}
sorp dual gyp disp CE	3.28×10^{6}

Sorption (sorp)

The initial testing of geochemical processes started with just the addition of sorption. Sorption was simulated in PHREEQC using the generic surface complexation approach presented by Davis et al. (2004). In this approach, uranium sorption is estimated using a generic sorption surface, and the estimated parameters are the uranium sorption surface equilibrium constants and the amount of sorption surface sites. Multiple uranium surface sorption equations can be used, but Davis et al. (2004) and Johnson et al. (2016a) found adequate results with just two equations, and the modeling for this report just used strong and super strong sorption sites with the uranyl ion (Appendix F has example file). Graphically, there is a good match between the simulated and measured uranium concentrations (Figure 25). However, the model-predicted concentrations of constituents such as calcium (Appendix F) and sulfate (Figure 26) are the same concentrations as of the influent solution, since no dissolution reactions are allowed.

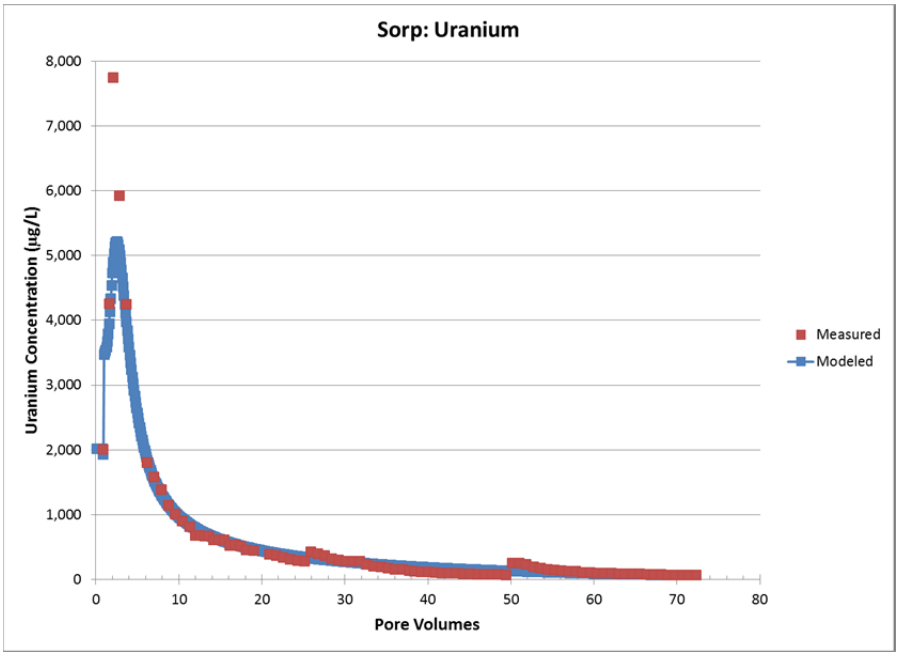

Figure 25. Measured and Modeled Uranium Concentrations for the Sorption-Only Model (sorp)

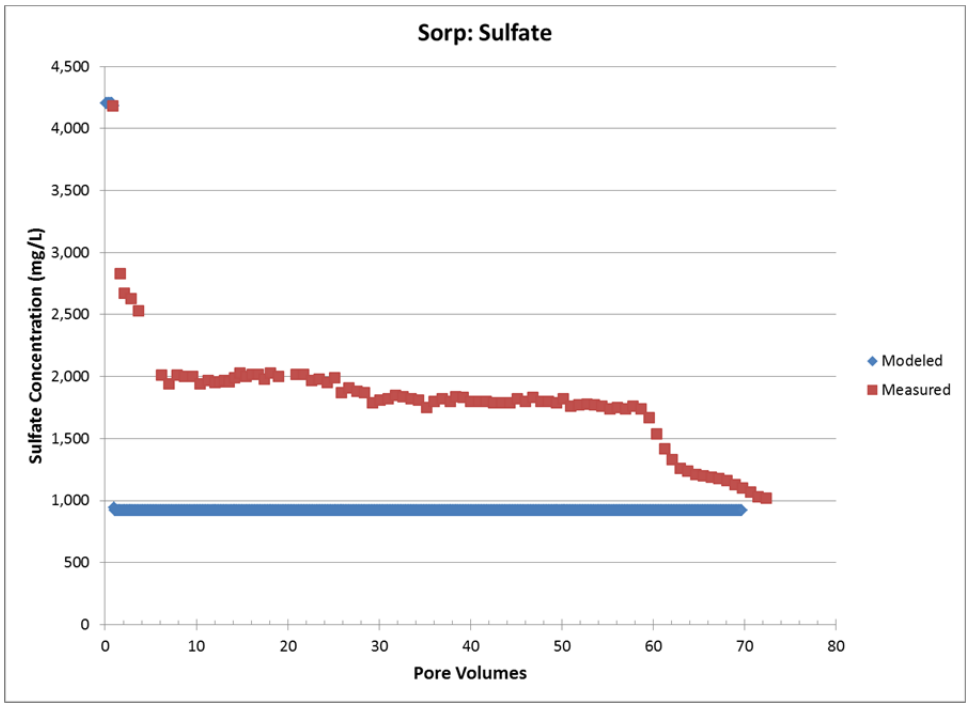

Figure 26. Measured and Modeled Sulfate Concentrations for the Sorption-Only Model (sorp)

Sorption and Dual Porosity (sorp dual)

The addition of dual porosity to sorption creates a slight improvement in the overall SOSWR value (Table 12) due to an improved fit to the stop-flow events that create a rebound affect for uranium (Figure 27), especially for the second stop-flow event. The addition of dual porosity is a reasonable added complexity based on the fission-track radiography and the evidence of uranium associated with intragranular cements. Thus, the addition of dual porosity in this case is adding a smaller porosity, slower groundwater flow rate in the intragranular cements compared to that of the surrounding sand and gravel aquifer with higher porosity and faster groundwater flow rates. However, other constituents such as calcium (Appendix F) and sulfate (Figure 28) still have a poor fit without the allowance for gypsum ($CaSO_4 \cdot H_2O$) dissolution.

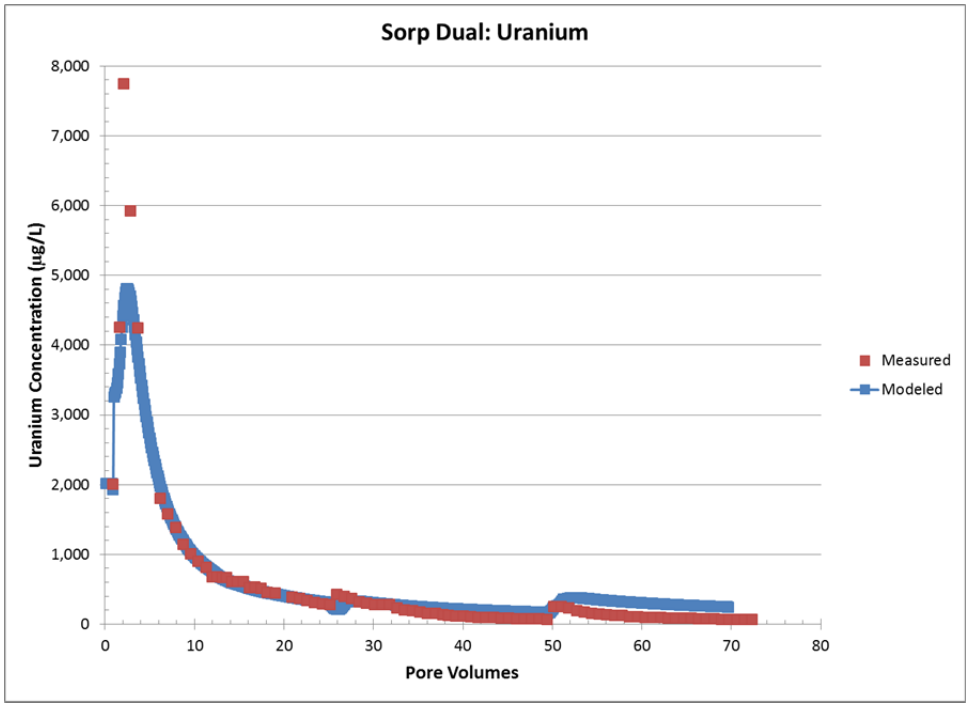

Figure 27. Measured and Modeled Uranium Concentrations for the Sorption and Dual Porosity Model

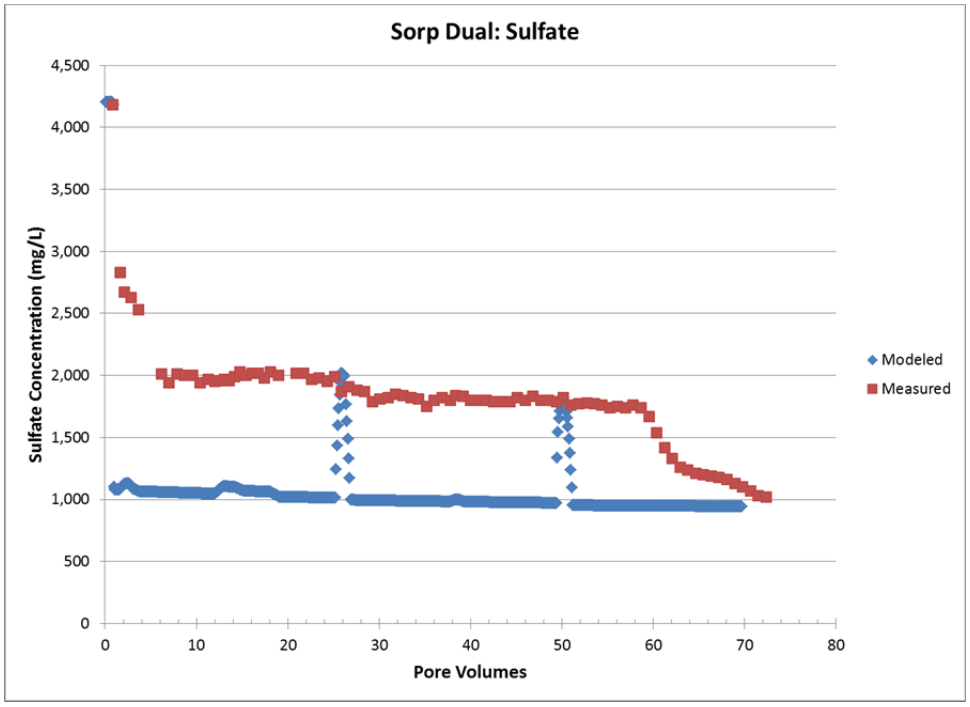

Figure 28. Measured and Modeled Sulfate Concentrations for the Sorption and Dual Porosity Model

Sorption and Gypsum (sorp gyp)

As mentioned above, the addition of gypsum dissolution is needed to provide a better calibration with calcium and sulfate. Before modeling sorption, dual porosity, and gypsum in combination, a model with just sorption and gypsum was tested for simplicity. With just sorption and gypsum equilibrium, the modeled uranium peak starts at a slightly smaller pore volume (Figure 29). The gypsum dissolution creates much improved calcium (Appendix F) and sulfate (Figure 30) matches, and the improved calcium and sulfate matches create an improved SOSWR from just using sorption and dual porosity (Table 12).

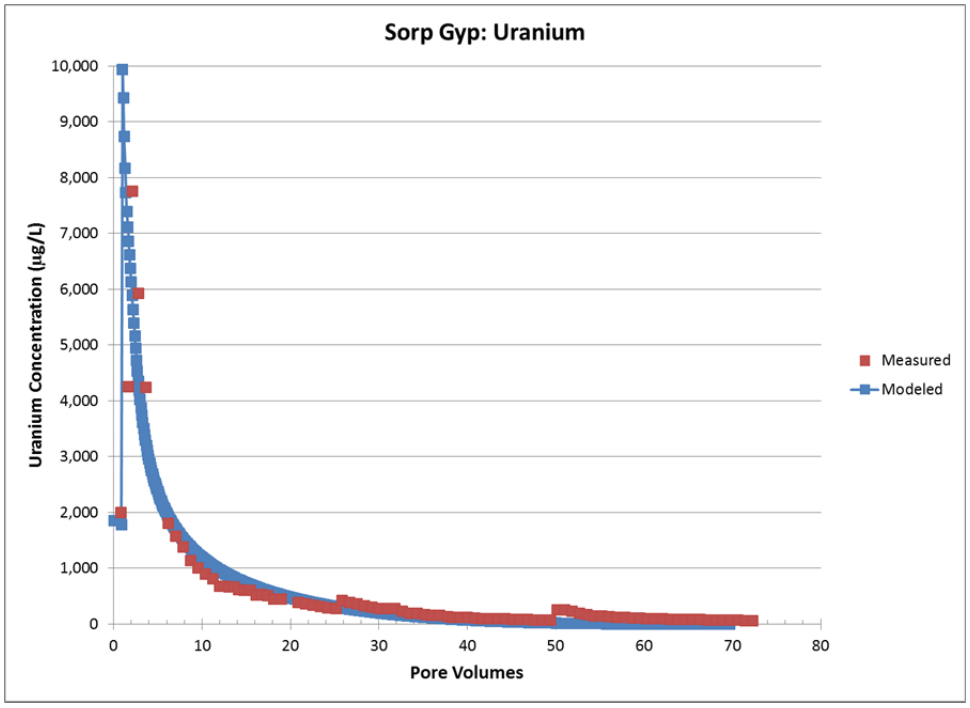

Figure 29. Measured and Modeled Uranium Concentrations for the Sorption and Gypsum Model (sorp gyp)

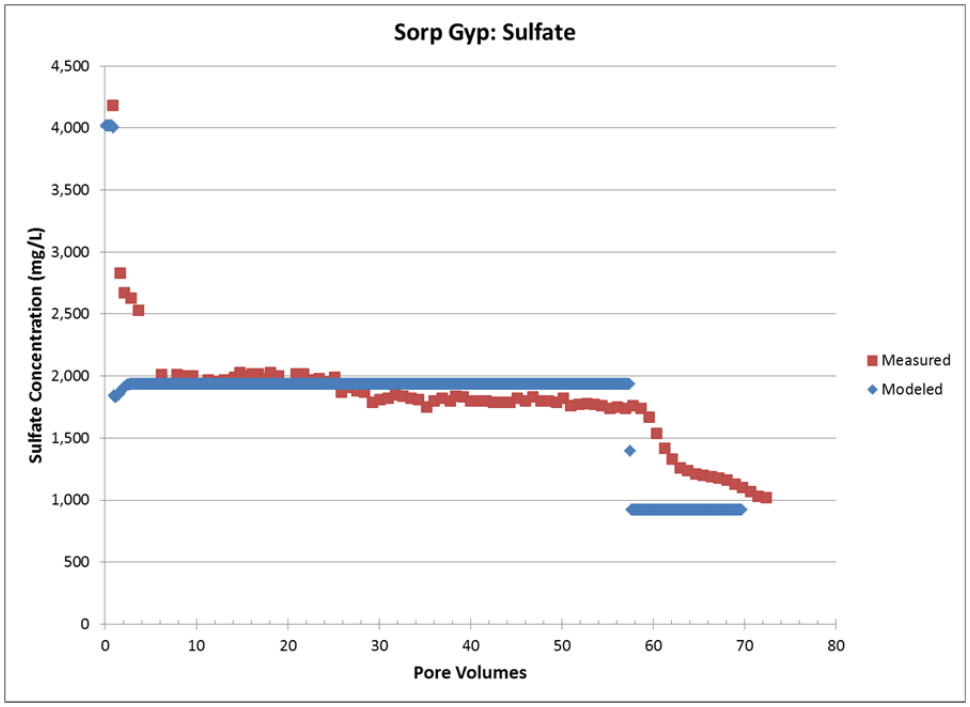

Figure 30. Measured and Modeled Sulfate Concentrations for the Sorption and Gypsum Model (sorp gyp)

Sorption, Dual Porosity, and Gypsum (sorp dual gyp)

The model simulation results presented above, with just sorption and then the addition of either dual porosity or gypsum, indicate that all three of these geochemical processes are important. In addition, the XRD identification of gypsum, and the fission-track identification of grains that likely have dual porosity combined with sorption to iron hydroxides, provides added empirical evidence that these processes are important.

The results for the sorption, dual porosity, and gypsum model are an improved SOSWR value of 1.01×10^7 (Table 12). However, in additional testing with different starting parameter values (Table 11), a second sorp dual gyp 2 model provided an even better fit with a SOSWR value of 3.61×10^6 (Table 12) This indicates that the calibration routine is likely finding a local minima before reaching a "true" best fit. In addition, the sorption parameters for the equilibrium constant and the number of sorption sites are inversely correlated, which means the calibration process can only find a ratio of these two values and not unique numbers. This complicates the model calibration and may exacerbate the local minima issue convergence issue. Unfortunately, it is difficult to avoid the issue of local minima without having additional a priori data on the parameter values (Doherty 2005), which is not available in this case.

This combined process model of sorp dual gyp and the revised starting parameters (presented here as sorp dual gyp 2) do provide an improved fit for all the measured constituents including uranium (Figure 31) and sulfate (Figure 32). Figure 33 shows the fit for uranium during the first stop-flow events. The modeled influence of dual porosity is more subdued that the measured influence, possibly because the majority of the calibration data is from pore volumes without any stop-flow events.

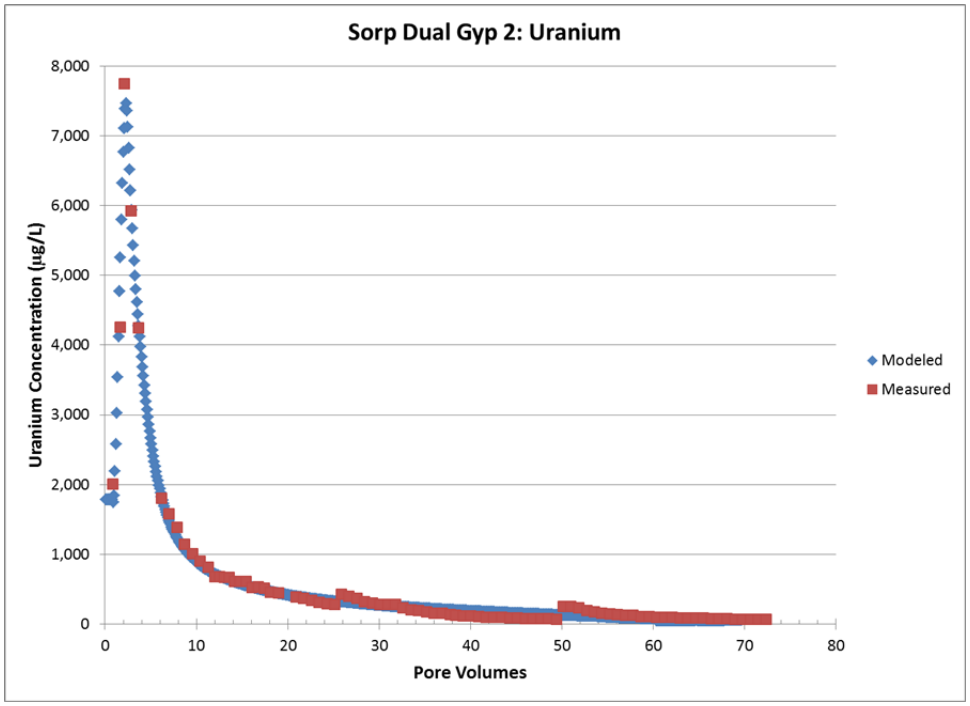

Figure 31. Measured and Modeled Uranium Concentrations for the Sorption, Dual Porosity, and Gypsum Model (sorp dual gyp 2)

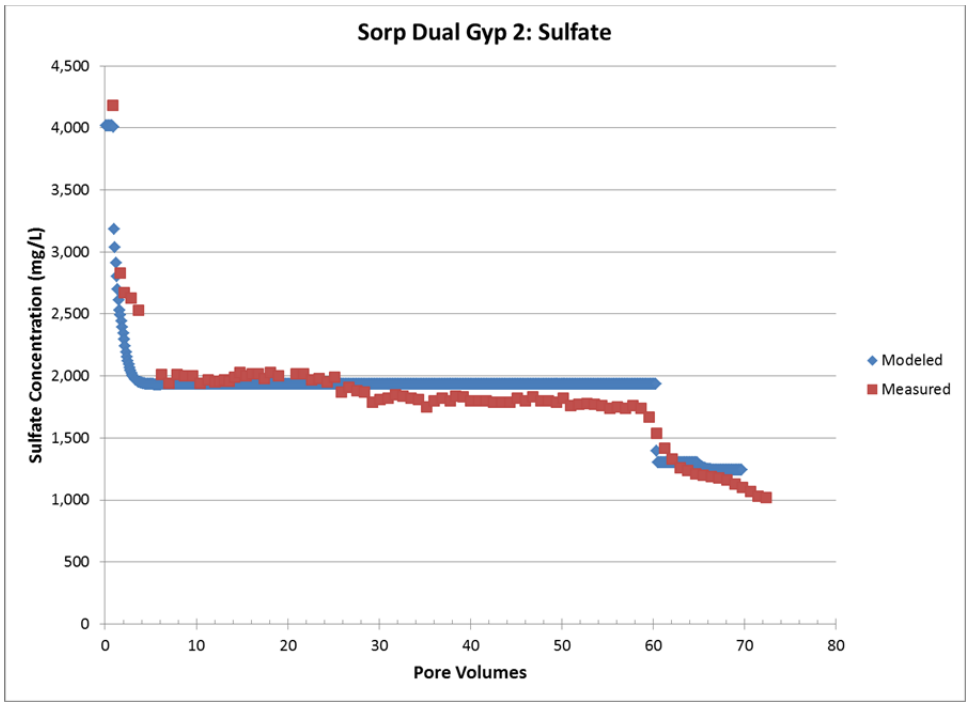

Figure 32. Measured and Modeled Sulfate Concentrations for the Sorption, Dual Porosity, and Gypsum Model (sorp dual gyp 2)

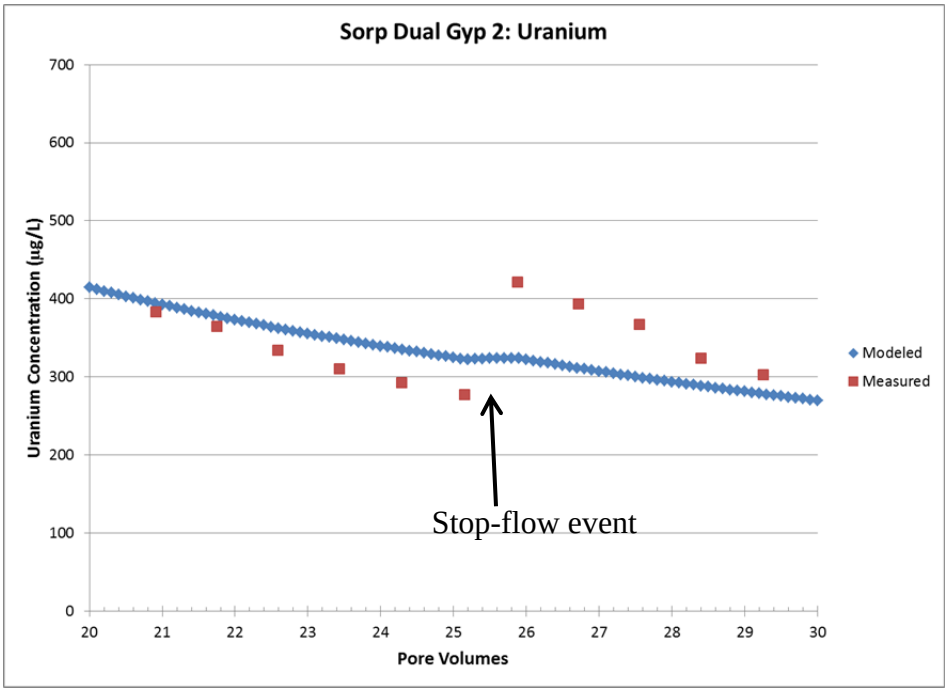

Figure 33. Measured and Modeled Uranium Concentrations for the Sorption, Dual Porosity, and Gypsum Model (sorp dual gyp 2) from 20 to 30 Pore Volumes

Sorption, Dual Porosity, Gypsum, and Calcite (sorp dual gyp calcite)

Calcite was added to the sorp dual gyp model because calcite is a reactive mineral (can precipitate and/or dissolve in a matter of hours or days) and can have a large influence on uranium mobility due to the formation of calcium uranyl carbonate complexes that keep uranium in solution. In addition, the XRD data indicated approximately 7% calcite by weight in the GJAST 20-10 sample. Calcite was added with a saturation index (SI) of 1.32, which was the median value calculated from the GJAST 20-10 column outflow data. The PHREEQC-calculated calcite SI for the influent solution was 0.1, indicating near-equilibrium conditions with respect to calcite. These SI values allowed for additional calcite dissolution within the model, and the effluent data indicate that calcite remained supersaturated, thus maintaining calcite dissolution above equilibrium conditions. However, only one measurement of pH and alkalinity was available for the influent solution in calculating the calcite SI. PHREEQC calculations indicate that the influent solution CO_2 concentrations with the measured pH and alkalinity were 100 times atmospheric CO_2 concentrations. With this condition, it is likely that CO_2 degassing was occurring during the column experiment, potentially before the influent solution reached the column. This may have created a pH value higher in the actual influent solution than that initially measured, thus creating uncertainty in quantitatively evaluating the influence of calcite dissolution.

The resulting SOSWR value for the sorp dual gyp calcite model was greater than that of the sorp dual gyp model (Table 12) because the simulations for the sorp dual gyp calcite model calculated a greater alkalinity (420 mg/L as $CaCO_3$) than was actually measured (variable, but near 300 mg/L as $CaCO_3$). This resulted in a much greater SOSWR value for alkalinity (Table F-2). In addition, the SOSWR value from the uranium measurements is 7.25 times greater in the sorp

dual gyp calcite model than in the sorp dual gyp 2 model. However, the simulated pH (near 7.7) in the sorp dual gyp calcite model water was similar to the measured column effluent pH near 7.9. By comparison, the model without calcite (sorp dual gyp 2) simulated alkalinity values (314 mg/L as $CaCO_3$) near the measured alkalinity values (variable, but near 300 mg/L as $CaCO_3$), but the simulated pH values of near 7 are quite a bit lower than the measured values near 7.9. This may have been due to the modeled input pH being too low, as discussed above. Since pH only varied between 7.5 and 8.2 in the column effluent and it is prone to measurement error that is transferred into geochemical modeling on a log scale, pH was not included as a calibration parameter and, thus, did not influence the overall SOSWR value.

While it is recognized that calcite dissolution can influence uranium mobility with the formation of calcium uranyl carbonate complexes (Dong and Brooks 2006), the addition of calcite to the sorp dual gyp model does not provide an improved fit to the measured data, except for pH. Possible pH measurement error and pH changes in the influent solution create uncertainty in evaluating the influence of calcite dissolution. However, the final results of the sorp dual gyp calcite simulations do not show an improvement in fitting the calibration data. In addition, the SI value for calcite of 0.1, or more if CO_2 was degassing and creating calcite supersaturation, in the influent solution makes it reasonable to assume that additional calcite dissolution should be minimal. Under different experimental conditions, if the influent solution was undersaturated with respect to calcite, calcite dissolution would need to be incorporated into the model as an added geochemical process that could also control uranium mobility.

Sorption, Dual Porosity, Gypsum, and Cation Exchange (sorp dual gyp CE)

Cation exchange on clays is very likely, as most aquifers have at least some clay present, and the XRD data for sample GJAST 20-10 did indicate 3% clays by weight. In PHREEQC, cation exchange is simulated by equilibrating the solid phase with the initial water chemistry. Similar to the simulations for sorption, the 0.83 PV solution (Table 6) was used as the initial solution for equilibrating the solid phase. The parameter being estimated is the number of moles of exchange sites (Table 10), which is essentially the amount of clay present in the solid phase. The preference for individual cations to sorb to the clays is controlled by selectivity constants provided in the selected database and the concentration of the cations in the solution (Parkhurst and Appelo 2013). The uranyl ion is not directly included as an exchangeable cation, but uranium mobility can be influenced by the concentration of Ca and Mg in solution, as these cations can form complexes with uranium carbonate species that keep uranium in solution (Dong and Brooks 2006).

The sorp dual gyp CE model produces the best SOSWR (Table 12), produces a good fit for uranium (Figure 34) with an even better rebound fit during the first stop-flow test (Figure 35) than the sorp dual gyp 2 model (Figure 33), and produces a better early-time sulfate fit (Figure 36) than the sorp dual gyp model (Figure 32). For uranium, neither the sorp dual gyp nor sorp dual gyp CE models provide a very good fit for the second stop-flow test at 50 volumes. The exact reason for this is unknown but is related to the final estimated dual porosity parameters (Table F1).

For the sorp dual gyp CE model, the magnesium fit at smaller pore volumes (Figure 37) is better than the magnesium fit at smaller pore volume in the sorp dual gyp 2 model (Figure 38). However, at larger pore volumes the magnesium concentration oscillates (Figure 37) and may

actually be overfitting the measured magnesium data, if the variations in magnesium data are slight differences that are within measurement error. Overall, based on the SOSWR and a qualitative visual comparison of the measured and modeled results (Figure 34 through Figure 37), the sorp dual gyp CE model is considered the best model for representing the measured column data. Indeed, sorption, dual porosity, gypsum dissolution, and cation exchange are all reasonable geochemical processes to include based on fission-track evidence of uranium sorption, thin sections that indicate dual porosity, and XRD data that detected 3% gypsum and clays by weight.

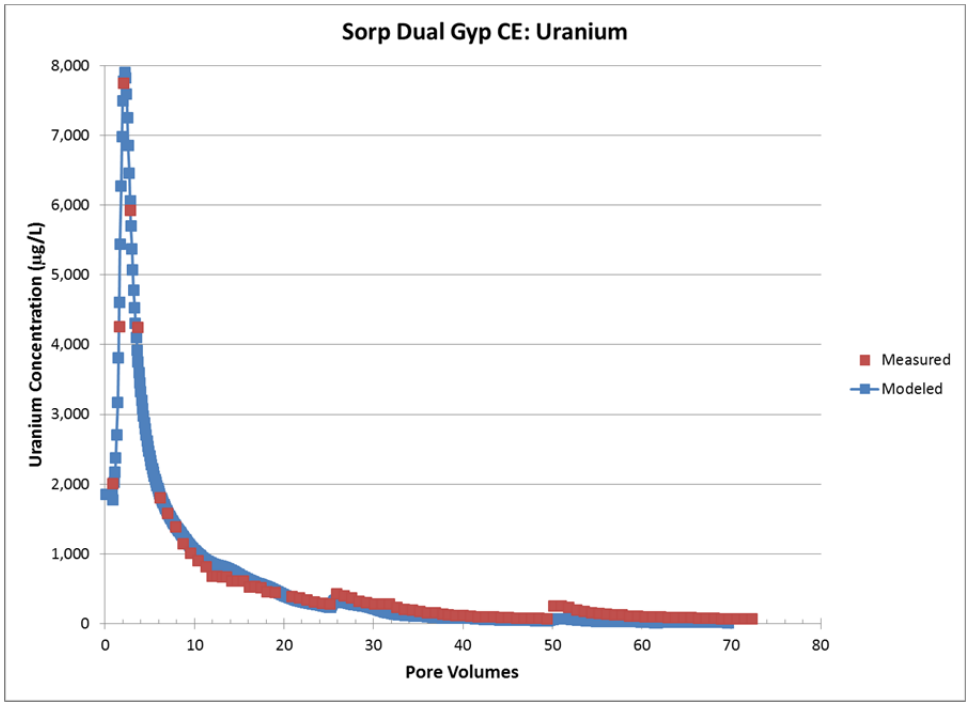

Figure 34. Measured and Modeled Uranium Concentrations for the Sorption, Dual Porosity, Gypsum, and Cation Exchange Model (sorp dual gyp CE)

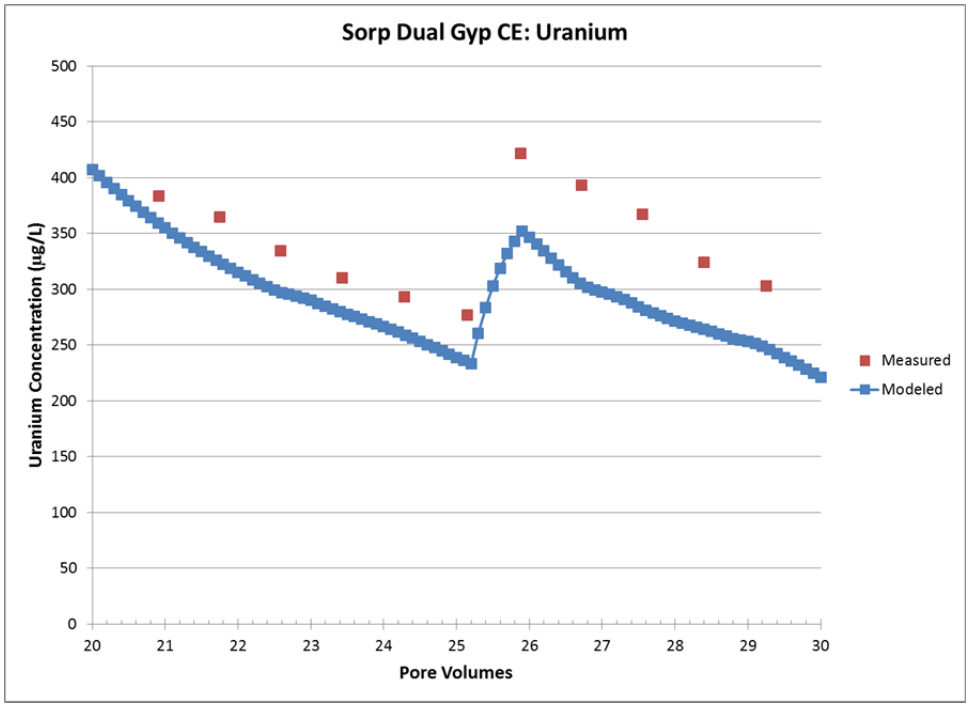

Figure 35. Measured and Modeled Uranium Concentrations for the Sorption, Dual Porosity, Gypsum and Cation Exchange Model (sorp dual gyp CE) from 20 to 30 Pore Volumes

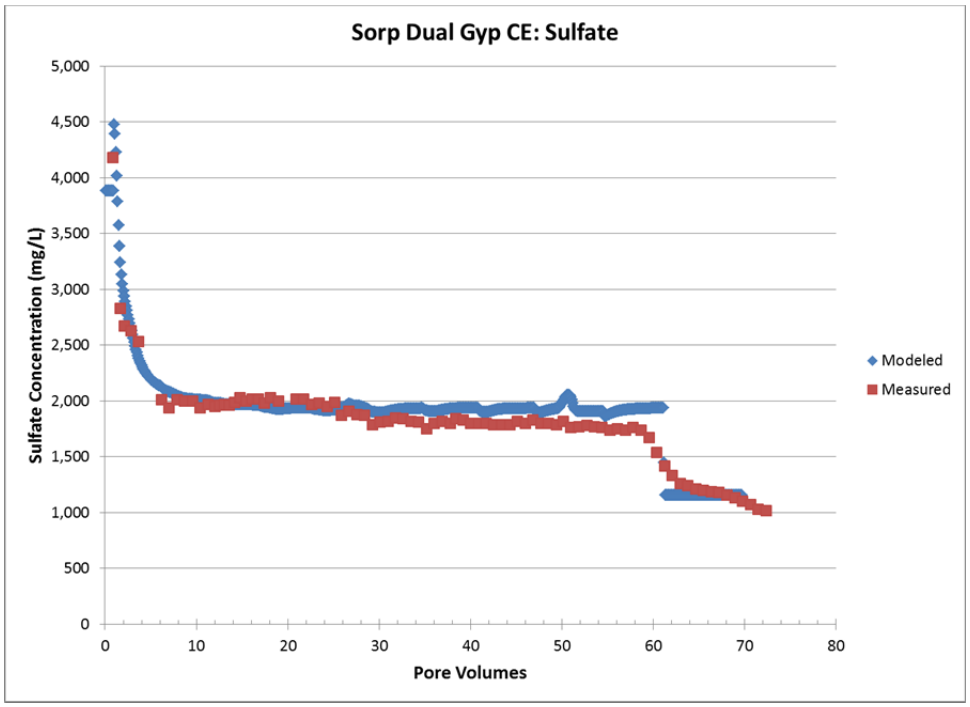

Figure 36. Measured and Modeled Sulfate Concentrations for the Sorption, Dual Porosity, Gypsum, and Cation Exchange Model (sorp dual gyp CE)

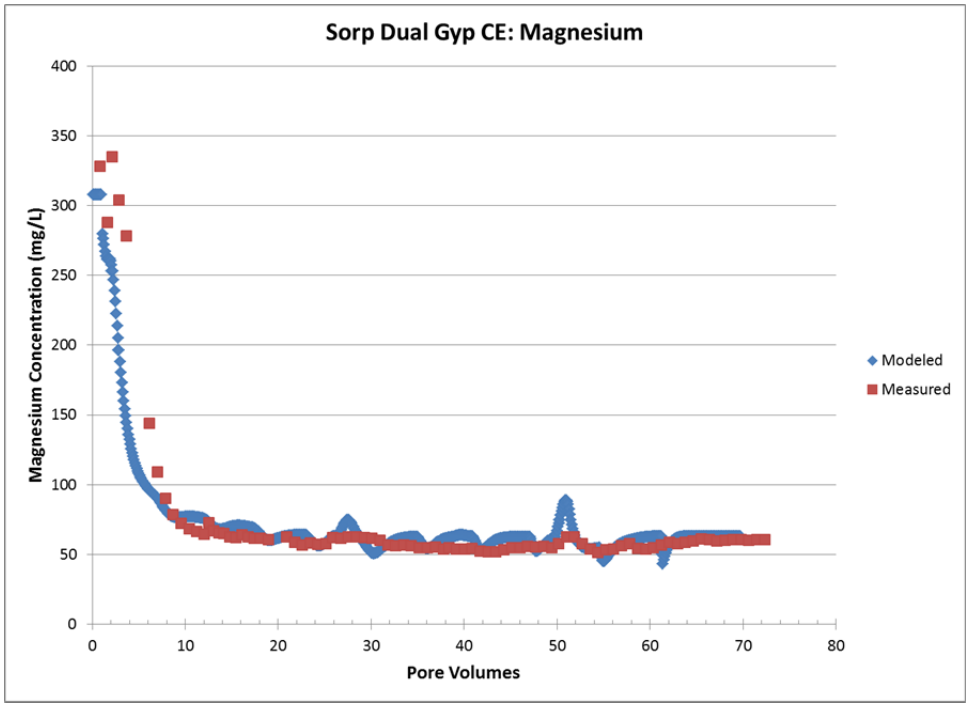

Figure 37. Measured and Modeled Magnesium Concentrations for the Sorption, Dual Porosity, Gypsum, and Cation Exchange Model (sorp dual gyp CE)

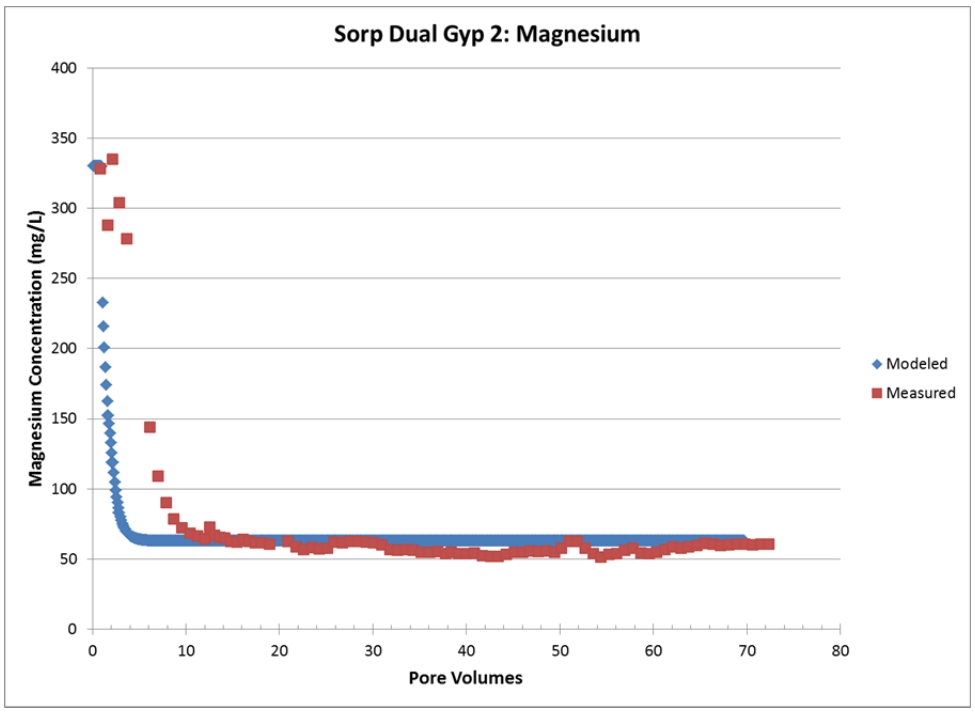

Figure 38. Measured and Modeled Magnesium Concentrations for the Sorption, Dual Porosity, and Gypsum Model (sorp dual gyp 2)

Sorp dual gyp disp

Dispersion is a common process in aquifers where contaminant concentrations are reduced due to heterogeneities encountered along the groundwater flow path. Albeit on a much smaller scale, the influence of dispersion was tested to see if this was an important process occurring within the column tests. Dispersion was added in the simulations of the GJAST-20-10 column tests by including a longitudinal dispersivity parameter (Table 10). The addition of dispersivity to the sorp dual gyp model produced a SOSWR value of 3.92×10^6, which is slightly worse that the sorp dual gyp 2 model at 3.61×10^6, but better than the sorp dual gyp model at 1.01×10^7 (Table 12). Thus, the inclusion of dispersivity does not appear to be an important process for the column tests, and results are within the convergence error of the sorp dual gyp model, likely due to local minima, as discussed before.

In addition, the model sensitivity to the dispersivity parameter is 3 orders of magnitude less than that of the other parameters (Appendix F, Table F-1). Thus, the importance of the dispersivity value to the model calibration is very minimal. Visual differences between the "sorp dual gyp" and "sorp dual gyp disp" models are difficult to distinguish (Appendix F).

Sorp dual gyp disp CE

The addition of dispersivity to the sorp dual gyp CE model resulted in a SOSWR value of 3.28×10^6, which is slightly worse that the original sorp dual gyp CE model at 3.10×10^6 (Table 12). In addition, the model sensitivity to the dispersivity parameter is 4 orders of magnitude less than the other parameters (Appendix F, Table F-1). Thus, the importance of the dispersivity value to the model calibration is very minimal. Visual differences between the sorp dual gyp CE and sorp dual gyp disp CE models results are difficult to distinguish (Appendix F).

While dispersion and the inclusion of dispersivity in field-scale models of uranium transport may be important, the use of dispersivity in the column test simulations appears to be unnecessary. The combination of a lack of improvement in the SOSWRs and low sensitivities in the results to dispersivity indicate that this process is not a valuable addition when simulating the geochemistry of the GJAST 20-10 column.

Flow Rates

In order for the column tests to be completed in a reasonable amount of time, column inflow rates are set much higher than the estimated groundwater flow rates in the field. For the GJAST 20-10 large column, the inflow target rate was 0.15 mL/min, which equates to a flow velocity of 1836 feet per year (ft/yr). The final sorp dual gyp CE model was rerun using a constant 1836 ft/yr flow velocity for 25 pore volumes. The original sorp dual gyp CE model had slight flow variations to match the measured column test data, but the targeted flow rate was 1836 ft/yr. The sorp dual gyp CE model was also rerun at a flow rate of 15 ft/yr, which is a more realistic groundwater flow rate for the Grand Junction site.

The simulated effluent uranium concentrations plotted against column pore volumes are relatively similar for both flow velocities (Figure 39). The main differences in the uranium concentrations are (1) the simulation with the 15 ft/yr velocity predicted a peak uranium concentration after a greater number of pore volumes, and (2) the simulation with the 1836 ft/yr

flow velocity maintains a higher uranium concentration at a greater number of pore volumes. The faster flow velocity simulation flushes the peak uranium concentration out of the column with fewer pore volumes but has a higher uranium concentration than the slower velocity simulation at greater than 10 pore volumes (Figure 39). Conceptually, this is created by the dual porosity mechanisms, which create nonequilibrium conditions with the higher velocity. This leads to initial flushing followed by a slow release of uranium from the less-mobile pores, requiring a greater number of pore volumes. This concept was tested in both flow velocities by adding a stop-flow test at 20 pore volumes. This resulted in rebound effects for the faster velocity simulation that were similar to the original column data, whereas the slower velocity simulation showed no effect from the stop-flow test. Overall, the simulations based on the final sorp dual gyp CE model indicate that dual porosity mechanisms seen in the column tests may be less important at the groundwater flow velocities that might be expected in the field.

When using pore volumes on the *x* axis, the simulation with the 1836 ft/yr flow velocity appears to have a slower uranium flushing rate. However, this can be misleading without looking at the time required to flush each pore volume at the different flow velocities. At the 1836 ft/yr flow velocity, it takes 200 minutes to flush a one-column pore volume, and at the 15 ft/yr flow velocity, it takes 24,480 minutes to flush a one-column pore volume. For comparison, to flush a simulated column to the 44 µg/L uranium standard, the faster flow velocity requires 53.3 pore volumes or 7.4 days (beyond the pore volumes shown on Figure 39), compared to the slower flow velocity requiring 23.7 pore volumes or 403 days. These results provide valuable quantitative information on the large numbers of pore volumes that are required to naturally flush uranium from contaminated sediment to the point that uranium in the effluent water is below standards.

Not surprisingly, the results above show that overall uranium flushing rates based on time do depend on water flow rates. However, faster flow rates appear to require more flushing on a pore volume basis if dual porosity mechanisms become important. This information could be applied to field scenarios if enhanced flushing is considered as a remedial strategy. In this case, simulations based on the column testing could be used to estimate required flushing times and the amount of water required (pore volumes). Future work may be required to confirm that this upscaling of the column test results to field conditions is actually valid.

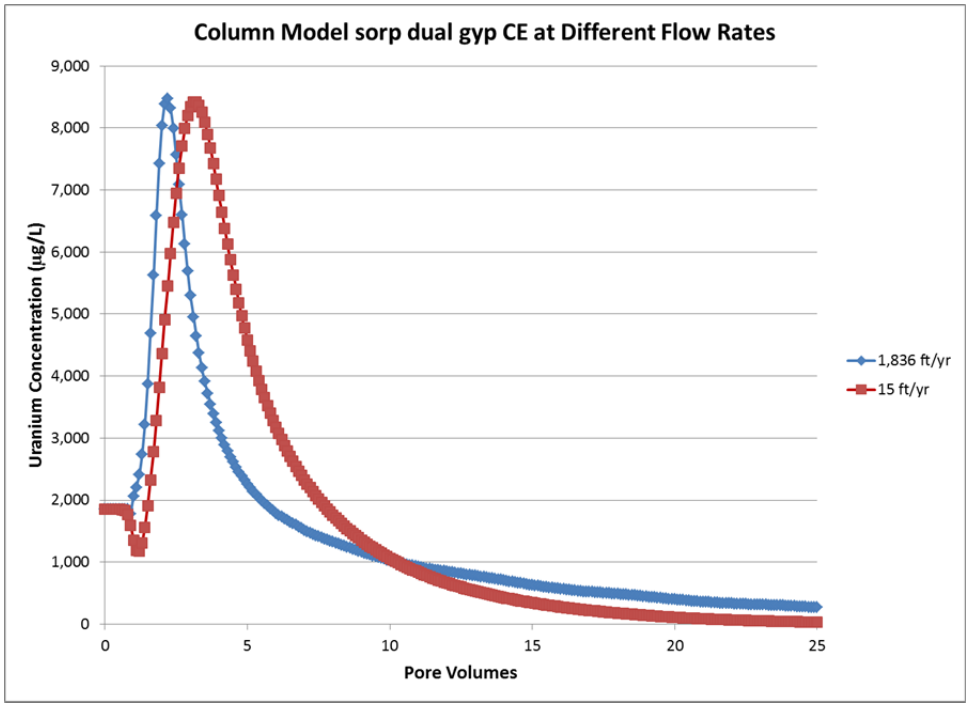

Figure 39. Simulated Uranium Concentrations for the Sorption, Dual Porosity, Gypsum, and Cation Exchange (sorp dual gyp CE) Model with Flow Rates of 1836 ft/yr (original targeted column test flow rate) and 15 ft/yr (more typical of groundwater flow rates)

5.0 Summary and Conclusions

The main study questions for this report are as follows:

5. How and where does uranium reside on the aquifer solids (i.e., uranium form and distribution)?
6. What are the uranium amounts and release rates from naturally aged aquifer solids?
7. What are the uranium release mechanisms?
8. How do the effects of questions 1–3 influence groundwater remediation strategies?

The adsorption of uranium on ferric oxyhydroxides is common in the shallow subsurface and is well understood under controlled laboratory conditions. This is an important process for the retention of uranium on the solid phase, thus leading to slow uranium release and plume persistence. Numerous studies have addressed uptake and release of uranium by adsorption and desorption on minerals. However, field conditions are much more complex, including possible sorption on other mineral surfaces and delayed desorption due to diffusion from less-mobile pore spaces (dual porosity).

This work focused on answering the study questions through detailed analyses of cores from 22 locations at the Grand Junction site. Although this work used site-specific data, many LM sites occur in similar settings on alluvial floodplains, and it is likely that the information from this report can be applied at other sites. Answering the study questions involved the use of selective chemical extractions (uranium amounts and where the uranium resides with depth),

fission-track radiography with thin-section petrography (how and where does uranium reside on the microscopic scale), X-ray diffraction (uranium association with mineralogy), column testing (uranium release rates), and reactive transport modeling (uranium release mechanisms and influence on groundwater remediation strategies).

5.1 Categorized by Study Questions

Question (1) How and where does uranium reside on the aquifer solid? The selective extraction data indicate that an increasing aggressiveness of the leaching/digesting solution increases the removal effectiveness of uranium from carbonate leach to 5% nitric acid leach, to microwave digestion, to total digestion. It is likely that the 5% nitric acid leach removes the majority of secondary uranium sorbed to mineral surfaces, whereas the total digestion provides a measurement of all uranium in the solid phase, and the microwave digestion effectiveness is between these two techniques. However, definitive association of the uranium associated with each selective extraction versus the mineralogy cannot be interpreted without post-extraction analyses.

Question (1) How and where does uranium reside on the aquifer solid? and Question (2) What are the uranium amounts? The selective extraction data show that zones with higher uranium concentrations at the site that have secondary uranium deposited due to the uranium mill processes can occur (1) above the water table (most common), (2) below the water table in limited areas and likely associated with gypsum, and (3) near and below the water table in association with organic carbon.

Question (1) How and where does uranium reside on the aquifer solid? Fission-track radiography indicates that uranium in the solid-phase samples is associated with (1) heavy mineral grains (i.e., monazites), (2) organic carbon, and (3) mineral coatings and cements. For mineral coatings and cements, the fission-track radiography indicates that uranium can be associated with intragranular material, likely composed of iron oxyhydroxides and/or clays. It is likely that a subtraction of 5% nitric acid leach uranium concentrations (uranium on mineral coatings and cements) from the total digestion uranium concentrations (all uranium) is equivalent to the uranium content found in the heavy mineral grains. These heavy mineral grains were deposited by the Gunnison River and contain naturally occurring uranium found within the mineral grains that is not related to uranium derived from the milling activities. This cannot be proven definitively without post-extraction analyses using fission-track radiography, but the primary uranium values at the site are similar to uranium crustal abundance values. Any remedial strategies should focus on the removal of excess uranium that was deposited by mill processes. Overall, any of the leach/extraction techniques can be used to determine the uranium content of contaminated material compared to background material for the amounts and locations of mill-related uranium added to the solid phase. However, the 5% nitric acid leach results provide results that are adequate for that determination without the other leach/extraction techniques. GJAST-03 and many of the samples below the water table at several boreholes appear to be representative of background uranium values that were likely present before the mill, based on data from three previous background samples collected upstream of the study area.

Question (2) What are the uranium amounts and release rates? Column tests data show an initial spike of uranium concentrations with the peak value correlating to the overall uranium content of the sample. After the peak concentration, uranium continues to be released, providing strong

evidence for possible plume persistence issues. The greatest uranium concentration peak was 6994 µg/L uranium from sample GJAST 14-8 at 2.5 pore volumes; the uranium concentration was approximately 400 µg/L at 9.5 pore volumes. The UMTRCA MCL for uranium of 44 µg/L was met after 36 pore volumes of flushing this sample with laboratory-prepared water that was similar in geochemistry to a nearby well.

Question (2) What are the uranium amounts and release rates? For the small columns, only uranium was measured in the outflow, so the geochemical controls are unclear. A larger column test was completed on sample GJAST 20-10 with complete geochemical measurements. For the larger column, the uranium trends were similar to the small column trends when plotted in relation to pore volumes, even with a slightly different flow rate. Data for calcium and sulfate indicate an increase in both of these constituents within the column due to gypsum dissolution. At the greater pore volumes, a decrease of calcium and sulfate concentrations at similar pore volumes is evidence of dissolution and depletion of the gypsum that was available in the column sample. Data from this larger column were used for reactive transport modeling and an evaluation of geochemical processes.

Question (3) What are the uranium release mechanisms? Reactive transport modeling tested a variety of geochemical process models to assess which processes were most important in controlling the release of secondary uranium from aquifer solids. This modeling provides information on the release of uranium that is controlled by pH, alkalinity, calcium, and magnesium that cannot be interpreted by just evaluating the column outflow data. Sorption and dual porosity proved to be the most important processes for calibrating the model to the column results. However, modeled sulfate and calcium concentrations were too low without the addition of gypsum to the model. The presence of gypsum was confirmed by XRD analysis. The modeling results showed a low sensitivity for dispersivity and some minor improvement with the addition of cation exchange. In addition, the modeling results indicate some nonuniqueness due to high parameter correlation and local minima during the parameter estimation process, as evidenced by different parameter starting values leading to different estimated parameter values. The effect of parameter correlation on predictive modeling for testing remedial strategies was beyond the scope of this study and will require further evaluation.

Question (4) How do the effects of questions 1–3 influence groundwater remediation strategies? Upscaling from column tests to the field scale is a difficult issue. Upscaling was tested with the final calibrated reactive transport model from the GJAST 20-10 large column test. The testing used the 1D column model, but with flow rates that are more representative of natural field conditions. At these slower groundwater velocities, the dual porosity influences seen in the actual column test do not exist. Using the column modeling results shows promise for an evaluation of overall flushing times and amount of water required (pore volumes) to compare alternative remediation strategies, but should be compared with actual field conditions and field testing before being applied. Remedial strategies that create faster groundwater flow velocities may be well represented by the original column testing with faster flow rates and concentration rebounds when the flow to the column is temporarily stopped.

6.0 Recommendations

This report provides information on how, where, and to what degree uranium resides on aquifer solids as determined by the use of selective extractions and fission-track radiography. When evaluating remedial strategies for uranium mill sites, thorough measurements of secondary uranium existing on the solid phase are necessary, as this uranium may be slowly released in the future, creating plume persistence issues. While the evaluation of the secondary uranium produced by mill processes can be done with the comparison of 5% nitric acid leach data to that of uncontaminated sediments, the addition of uranium-234/uranium-238 isotope activity ratios on the nitric acid leach solution has the potential to distinguish how much of the secondary uranium is derived from mill-related versus non-mill-related sources.

The fission-track radiography data do provide information on how and where uranium resides on a microscopic scale. For the purposes of remedial strategies, uranium-associated organic carbon and the mineral coatings and cements are the most significant factors, as this is where uranium is most easily sorbed, desorbed, or precipitated. In turn, these microscopic structures control the uranium release rates during natural flushing or active remedial strategies. This report gives general information on these solid-phase controls on uranium, but more-detailed information will be necessary to truly evaluate and provide predictions of uranium release rates. Additional work will be necessary to determine how the presence of gypsum and iron oxyhydroxides in combination may control the release of uranium as the gypsum dissolves. Both gypsum and iron oxyhydroxides are common precipitation products as mill-related waters are buffered and become oxidized. It is still unclear whether one or both minerals tend to incorporate uranium. After the ground surface is remediated, incoming water with less dissolved constituents begins to dissolve the gypsum and desorb uranium from the iron oxyhyroxide surfaces. Evaluation of these processes will likely require unique analytical methods. In addition, more work will be necessary to understand if the presence of organic carbon provides a long-term source or sink for secondary uranium.

While this report provides general uranium release rates from column testing, uncertainties in upscaling to field conditions still exist. Tracer testing is a tool that can be used at the field scale to evaluate all the same processes that were seen in the column tests (sorption, dual porosity, dissolution/precipitation reactions, and cation exchange). Tracer testing can be completed by injecting multiple tracers with different geochemical properties and monitoring their mobility under natural or forced gradients. The results can then be simulated in reactive transport models with procedures similar to those presented here. This will allow for a field-scale evaluation of various geochemical processes and provide calibrated parameter input values derived from the field. A comparison of the calibrated model parameters from column simulations to field-scale simulations can be used to assess scale and flow velocity effects. The calibrated parameter values from a field-scale model are then used to test multiple remediation strategies through modeling before being implemented, with the potential for large cost savings. Although the field testing will likely include just one geochemical condition (i.e., pH, alkalinity, etc.) due to the cost of setting up a field test, additional column testing can be completed to test various input fluids that might be useful for remedial strategies that influence uranium mobility.

If it is determined that additional site-specific information is needed to enhance remedial action treatability studies or to support changing a site compliance strategy, the following list summarizes recommended procedures for evaluating plume persistence issues at a site:

9. Make a thorough evaluation of existing mill-related uranium on the solid phase with depth.
10. Use microscopic techniques to determine where and how the uranium exists in the solid phase in association with the mineralogy.
11. Use tracer tests with companion column tests to determine contaminant release rates and mobility, which may include testing various influent fluids.
12. Calibrate reactive transport models using the data from recommendation 3 to get realistic input parameters. This step should include the evaluation of parameter sensitivities and uncertainties.
13. Use reactive transport models with the final input parameters derived from recommendation 4 to evaluate flushing rates and test various remedial strategies (such as targeted injection areas with different influent solution chemistry). This step should include an evaluation of prediction uncertainties using sensitivity analyses.

All the above recommendations have been incorporated in a new AS&T Technical Task Plan titled *Persistent Secondary Contaminant Sources*. This follow-on TTP will provide generic guidance that can be used at any LM site to follow the five steps listed above when evaluating plume persistence issues and determining appropriate remedial strategies.

7.0 References

Ames, L.L., J.E. McGarrah, and B.A. Walker, 1983. Sorption of trace constituents from aqueous solutions onto secondary minerals I. uranium, *Clays and Clay Minerals* 31:321–334.

Davis, J. A., and J.O. Leckie, 1978. Surface ionization and complexation at the oxide/water interface ii. surface properties of amorphous iron oxyhydroxide and adsorption of metal ions, *Colloid and Interface Science* 67:90–107.

Davis, J.A., D.E. Meece, M. Kohler, and G.P. Curtis, 2004. Approaches to surface complexation modeling of uranium(VI) adsorption on aquifer sediments, *Geochimica et Cosmochimica Acta* 68:3621–3641.

DOE (U.S. Department of Energy), 1989. *Final Remedial Investigation/Feasibility Study for the U.S. Department of Energy Grand Junction (Colorado) Projects Office Facility*, DOE/ID/12584-16, UNC-GJGRAP-1, Grand Junction Projects Office, Grand Junction, Colorado, April.

DOE (U.S. Department of Energy), 1995. *Final Report of the Decontamination and Decommissioning of the Exterior Land Areas at the Grand Junction Projects Office Facility*, DOE/ID/12584-220, GJPO-GJ-13, Grand Junction Projects Office, Grand Junction, Colorado, September.

DOE (U.S. Department of Energy), 2002. *Long-Term Surveillance and Maintenance Program Sediment Sampling and Analysis Report for the Grand Junction, Colorado, Office Facility*, GJO-2002-288-TAR, GJO-LGJO 6.3-2, Grand Junction Projects Office, Grand Junction, Colorado, November.

DOE (U.S. Department of Energy), 2016. *Fact Sheet for the Grand Junction, Colorado, Site*, November, http://www.lm.doe.gov/Grand_Junction/Fact_Sheet_GJO.pdf

Doherty, J., 2005. *PEST, Model-Independent Parameter Estimation User Manual*, 5th ed, Watermark Numerical Computing.

Dong, W. and S.C. Brooks, 2006. Determination of the formation constants of ternary complexes of uranyl and carbonate with alkaline earth metals (Mg^{2+}, Ca^{2+}, Sr^{2+}, and Ba^{2+}) using anion exchange method, *Environmental Science & Technology* 40:4689–4695.

Dzombak, D.A. and F.M.M. Morel, 1990. *Surface Complexation Modeling*, Wiley & Sons, New York.

Guillaumont, R., T. Fanghanel, J. Fuger, I. Grenthe, V. Neck, D. Palmer, and M.H. Rand, 2003. *Update on the Chemical Thermodynamics of Uranium, Neptunium, Plutonium, Americium, and Technetium*, Elsevier, Amsterdam.

Henwood, P., and C. Ridolfi, 1986. *Radiologic Characterization of the Department of Energy Grand Junction Project Office*, GJ-41. Bendix Field Engineering Corporation, Grand Junction Operations, U.S. Department of Energy, Grand Junction Projects Office.

Hsi, C.D. and D. Langmuir, 1985. Adsorption of uranyl onto ferric oxyhydroxides: application of the surface complexation site-binding model, *Geochimica et Cosmochimica* 49:1931–1941.

Johnson R.H., R. Truax, D. Lankford, and J. Stone, 2016a. Sorption testing and generalized composite surface complexation models for the determination of uranium sorption parameters at a proposed uranium in situ recovery site, *Mine Water and the Environment*, DOI 10.1007/s10230-016-0384-6.

Johnson, R., S. Morrison, S. Morris, A. Tigar, W.L. Dam, and J. Dayvault, 2016b. Column Testing and 1D Reactive Transport Modeling to Evaluate Uranium Plume Persistence Processes, in *IMWA 2016 – Mining Meets Water – Conflicts and Solutions*, Drebenstedt, C. and Paul, M. Eds., pp. 652–659; Freiberg/Germany (TU Bergakademie Freiberg), http://www.imwa.info/docs/imwa_2016/IMWA2016_Johnson_20.pdf.

Ledger, E.G., B.J. Bomber, W.E. Schaftenaar, and T.T. Tieh, 1984. Uranium occurrence in major rock types by fission-track mapping, *American Association of Petroleum Geology Bulletin*, 68(4):499.

McGinley, F.E., 1987. *Historical Survey of the Grand Junction Projects Office Facility – Hazardous (non-radioactive) Wastes*, prepared for UNC Technical Services, Inc. P.O. No. 26551.

Morrison, 2016. S. J. Morrison, geochemist with Navarro Research and Engineering, Inc., telephone conversation with R.H. Johnson, Navarro Research and Engineering, Inc., June 15.

Morrison, S.J., R.R. Spangler, and V.S. Tripathi, 1995. Adsorption of uranium(VI) on amorphous ferric oxyhydroxide at high concentrations of dissolved carbon(IV) and sulfur(VI), *Journal of Contaminant Hydrol*ogy 17:333–346.

Parkhurst, D.L. and C.A.J. Appelo, 2013. Description of input and examples for PHREEQC version 3--A computer program for speciation, batch-reaction, one-dimensional transport, and inverse geochemical calculations: *U.S. Geological Survey Techniques and Methods*, Book 6, Chapter A43, http://pubs.usgs.gov/tm/06/a43/.

Schwertmann, U. and R.M. Cornell, 1991. *Iron Oxides in the Laboratory*, VCH, Weinheim.

Smith, B.F.L. and B.D. Mitchell, 1987. In: *A Handbook of Determinative Methods in Clay Mineralogy*, Blackie, Glasgow, pp. 275–294.

Taylor, S.R., 1964. Abundance of chemical elements in the continental crust; a new table, *Geochimica et Cosmochimica Acta* 28(8):1273–1285.

Tripathi, V.S., 1984. *Uranium(VI) Transport Modeling: Geochemical Data and Submodels*, PhD Dissertation, Stanford University.

Zielinski, R.A., J.K. Otton, R.R. Schumann, and L. Wirt, 2007. *Uranium in Surface Waters and Sediments Affected by Historic Mining in the Denver West 1:100,000 Quadrangle, Colorado*, U.S. Geological Survey Scientific Investigation Report 2007-5246.